INVESTIGATING SUBSTRATE DISCRIMINATION BY THE FISSION YEAST LA PROTEIN DURING STRESS

VANESSA SINAGOGA

A THESIS SUBMITTED TO THE FACULTY OF GRADUATE STUDIES
IN PARTIAL FULFILLMENT OF THE REQUIREMENTS FOR THE DEGREE OF

MASTER OF SCIENCE

GRADUATE PROGRAM IN BIOLOGY
YORK UNIVERSITY
TORONTO, ONTARIO

August 2023

ABSTRACT

The La protein is an RNA-binding protein first identified as an autoantigen in Lupus patients. La's best characterized function is to protect the 3' end of pre-tRNAs from degradation by binding their characteristic UUU-3'OH tails. La also facilitates pre-tRNA folding through a poorly understood RNA chaperone mechanism. We hypothesized that the *Schizosaccharomyces pombe* La protein (Sla1p) discriminates among RNA substrates based on fold, selectively binding misfolded RNAs for chaperone intervention during cellular stresses predicted to disrupt RNA structure. High-throughput sequencing of Sla1p-associated RNAs did not reveal altered interaction between Sla1p and pre-tRNAs during stress, suggesting a lack of substrate discrimination by Sla1p. Northern blotting revealed novel perturbations to pre-tRNA processing in *S. pombe* during oxidative stress and nutrient starvation. Overall, this work has added to our understanding of La's chaperone activity, and seeded future work toward uncovering further details of stress-dependent alterations to pre-tRNA processing in fission yeast.

This thesis is dedicated to the memory of my Zia (aunt) Anna,
who was like a second mother to me.

Her strength, perseverance, and faith through life's hardest challenges
will always serve as the greatest of the many lessons she taught me.

ACKNOWLEDGEMENTS

To my supervisor, Dr. Mark Bayfield: thank you for your continuous support and guidance through the craziness that is grad school. I truly could not have asked for a better supervisor to see me through this journey. Thank you for your excitement for this project, for your belief in me (especially when my own belief in myself faltered), and for making the lab an enjoyable space. Most importantly, thank you for your unwavering support and understanding during my cancer diagnosis and treatment.

To Dr. Kathi Hudak: I was lucky enough to have been able to learn from you since undergrad. Your attention to detail, patience, and desire to help students understand are truly admirable. Thank you for your insightful feedback during progress report meetings, and making those meetings feel as comfortable as possible. Thank you also to Dr. David Hood and Dr. Emanuel Rosonina for lending your time to serve on my thesis committee.

Thank you to the amazing members of the Bayfield Lab for teaching me so much and for making the lab feel like a family. As your scientific careers take you far and wide, I know we will remain friends! To Farnaz: I am incredibly grateful for your mentorship over the years. Thank you for your words of wisdom as I contemplated if grad school was right for me, and for literally being a shoulder to cry on. To Jennifer: Thank you for insisting that my constant questions in the lab weren't annoying! Thank you for always reassuring me during bouts of anxiousness, and for all your help inside and outside of the lab. To Kyra: Thank you for all the laughs over the years and encouragement during experiments and thesis writing. To Connor and Brittney: Although our

time in the lab together didn't overlap much, I'm very grateful for the time and space we shared.

Thank you to all our collaborators at L'Université de Sherbrooke, especially Étienne Fafard-Couture, for helping us collect great data and for navigating the intimidating world of RNA sequencing data analysis.

Finally, to my family:

To Zia Laura and my cousin, Gabby: Thank you for providing some much-needed comic relief, and for all your support and encouragement over these challenging years.

To my parents and younger brother, Nicholas: I am certain that this journey (especially the last year) would have been much more difficult without you by my side. Thank you for pushing me to be my best while reminding me that I am the captain of my own ship. None of this would be possible without your unwavering love and support!

TABLE OF CONTENTS

LIST OF FIGURES

CHAPTER 1: INTRODUCTION

CHAPTER 2: MATERIALS AND METHODS

CHAPTER 3: RESULTS

APPENDIX A

LIST OF TABLES

APPENDIX A

LIST OF ABBREVIATIONS

^{32}P	Phosphorus-32
8-OHG	8-hydroxyguoanosine
Asn	Asparagine
ATP	Adenosine triphosphate
bp	Base pair
BSA	Bovine serum albumin
cat. #	Catalogue number
cDNA	Complementary DNA
ChIP	Chromatin immunoprecipitation
CPM	Counts per million
CTD	C-terminal domain
ddH_2O	Double distilled water
DNA	Deoxyribonucleic acid
DTT	Dithiothreitol
E. coli	*Escherichia coli*
ECL	Enhanced chemiluminescence
EDTA	Ethylenediaminetetraacetic acid
EMM	Edinburgh minimal media
EtBr	Ethidium bromide
FT	Flow-through
g	Force of gravity
H_2O_2	Hydrogen peroxide
HCl	Hydrochloric acid
HEPES	4-(2-hydroxyethyl)-1-piperazineethanesulfonic acid
His	Histidine
HRP	Horse radish peroxidase
IgG	Immunoglobulin G
Ile	Isoleucine
IP	Immunoprecipitation
IPTG	Isopropyl-β-D-1-thiogalactopyranoside
kDa	Kilodalton
KOAc	Potassium acetate
LAM	La motif
LARP	La-related protein
LB	Lysogeny broth
LiAc	Lithium acetate

log	Logarithm
Lys	Lysine
mRNA	Messenger RNA
NaCl	Sodium chloride
NaOAC	Sodium acetate
ncRNA	Non-coding RNA
NP40	Nonyl phenoxypolyethoxylethanol
NTD	N-terminal domain
OD	Optical density
OH•	Hydroxyl free radical
PBS	Phosphate-buffered saline
PEG	Polyethylene glycol
PIC	Protease inhibitor cocktail
PMSF	Phenylmethylsulfonyl fluoride
PNK	Polynucleotide kinase
PrA	Protein A
pre-tRNA	Precursor tRNA
PVDF	Polyvinylidene difluoride
PVP40	Polyvinylpyrrolidone 40
qRT-PCR	Quantitative reverse transcriptase polymerase chain reaction
RIP	RNA immunoprecipitation
RNA	Ribonucleic acid
RNAP	RNA polymerase
RNase	Ribonuclease
RNP	Ribonucleoprotein
RoR	Ratio of ratios
rpm	Revolutions per minute
RRM	RNA recognition motif
rRNA	Ribosomal RNA
RTD	Rapid tRNA decay
S. pombe	*Schizosaccharomyces pombe*
S2U	Thiolation of uridine
SDS-PAGE	Sodium dodecyl sulfate-polyacrylamide gel electrophoresis
SEM	Standard error of the mean
Seq	Sequencing
Ser	Serine
Sla1p	*S. pombe* La protein
snRNA	Small nuclear RNA

snRNP	Small nuclear ribonucleoprotein
SSC	Saline sodium citrate
Stat.	Stationary phase stress
TBS	Tris-buffered saline
TGIRT	Thermostable group II intron reverse transcriptase
T_m	Melting temperature
TRAMP	*Trf4/5, Air1/2, Mtr4*, polyadenylation complex
Tris	Tris(hydroxymethyl)aminomethane
Trm1p	tRNA methyltransferase 1
tRNA	Transfer RNA
TSS	Transcription start site
Tyr	Tyrosine
Ura	Uracil
UV	Ultraviolet
Val	Valine
WT	Wild type
YES	Yeast extract with supplements

CHAPTER 1: INTRODUCTION

The extensive array of RNA molecules in the eukaryotic cell allude to their involvement in the intricate mechanisms of gene expression. Specifically, cells contain two major functional classes of RNAs: those that encode proteins, often called 'coding' or messenger RNAs (mRNAs), and functional non-coding RNAs (ncRNAs) that aid in the expression of mRNAs, among other biological processes. Post-transcriptional regulatory processes are controlled by well-characterized RNA-protein interactions through the formation of ribonucleoprotein (RNP) complexes. For example, small nuclear RNAs (snRNAs) assemble into small nuclear ribonucleoproteins (snRNPs) and together function in the splicing of mRNAs (Lerner & Argetsinger Steitz, 1979). Additionally, ribosomal RNAs (rRNAs) associate with ribosomal proteins in the cytoplasm to form the ribosome, the cellular machine responsible for protein translation. Importantly, transfer RNAs (tRNAs) function as adapter molecules during translation by decoding the mRNA and supplying the ribosome with the appropriate amino acid. Even beyond protein translation, ncRNAs are often implicated in RNPs for their own maturation. Of particular interest in this work are tRNA-containing RNP complexes.

1.1 RNA chaperone proteins solve the RNA folding problem

The regulatory mechanisms mentioned above are heavily influenced by the dynamic nature of RNA structure. As is the case with any other biological molecule, the three-dimensional structure of RNA is intimately related to its function. In comparison to proteins,

whose primary structure is composed of 20 possible amino acids, RNA exhibits a scarcity of primary structure diversity, with only four possible nitrogenous bases, as well as an overall structural similarity between these bases (Doetsch et al., 2011; Herschlag, 1995). As a result, the structural diversity observed in RNA is mediated by secondary and tertiary interactions. Secondary structure is driven by traditional Watson-Crick, and G-U base pairing in regions of complementarity, while additional hydrogen bonding and base stacking facilitate tertiary structure (Draper, 1992). As a result, the folding of RNA is not only a slow process but one that results in multiple, biologically inactive secondary structures from a single sequence (Doetsch et al., 2011).

The requirement for RNA molecules to exist in their native conformation is widely regarded as the 'RNA folding problem' and is described as two-fold: a kinetic problem, and a thermodynamic problem (Russell, 2008). The kinetic problem describes the propensity of nascent RNAs to be kinetically trapped in a non-functional conformation. The thermodynamic problem lies within the challenge of the functional RNA structure to outcompete alternate structures in thermodynamic stability (Russell, 2008). Compared to *in vitro* environments, RNA folding *in vivo* has been shown to be more efficient due to the availability of RNA-binding proteins that facilitate in their folding (Rajkowitsch et al., 2007). Specifically, a class of RNA-binding proteins called RNA chaperones help solve the RNA folding problem by decreasing the energy barrier required for the transition from kinetic traps to a correctly folded structure (Draper, 1992; Rajkowitsch et al., 2007).

RNA chaperones encompass a wide variety of proteins that do not share a common motif or structure but are similar in their ability to promote the native fold of RNA molecules in the absence of an energy input (ie. ATP hydrolysis) (Rajkowitsch et al., 2007). Consistent with their role of binding negatively charged RNA, RNA chaperone proteins tend to be basic, with increased proportions of arginine (Russell, 2008). Additionally, many RNA chaperone proteins contain regions with high intrinsic disorder that are predicted to facilitate rapid association and dissociation with substrates, as well as provide flexibility to bind a wide range of targets (Ivanyi-Nagy et al., 2008; Rajkowitsch et al., 2007). Binding of RNA chaperones to misfolded RNAs occurs with low specificity. This, along with the notion that natively folded RNAs are more thermodynamically stable than chaperone bound RNAs, suggest that chaperones interact transiently with their RNA substrates (Rajkowitsch et al., 2007). Although RNA chaperones have been well characterized with respect to their RNA binding ability, detailed mechanisms of their action remain ambiguous (Rajkowitsch et al., 2007; Vakiloroayaei et al., 2017). The current general model of RNA chaperone activity depicts weak and transient binding with misfolded RNAs, resulting in the destabilization of the intermediate fold. An accompanying decrease in free energy between the intermediate and native fold drives the formation of the native structure. The chaperone then releases the functional RNA, and associates with a different misfolded target (Doetsch et al., 2011). Overall, repeated cycles of chaperone-induced unfolding and refolding provide the substrate with many opportunities to fold correctly (Woodson et al., 2018).

1.2 The La protein

First identified as an autoantigen in patients with systemic lupus erythematosus and Sjogren's syndrome, La proteins are ubiquitous, eukaryotic RNA-binding proteins with characterized RNA chaperone function (Chakshusmathi et al., 2003; Chan et al., 1989; Huang et al., 2006; Mattioli & Reichlin, 1974). La is essential in humans and other higher eukaryotes (Park et al., 2006), while its dispensability in lower eukaryotes drives much of the present research surrounding its chaperone activity. Genuine La proteins belong to the larger family of La-related proteins (LARPs) that possess both conserved and divergent structure and functions in comparison to La (Maraia et al., 2017).

As with many other RNA-binding proteins, La is modular (**Figure 1.1**), yet also contains regions of intrinsic disorder. Genuine La proteins have highly conserved N-terminal domains (NTDs). Characteristic of La protein NTDs is the La module, a region consisting of the conserved La motif (LAM) and RNA recognition motif (RRM) separated by a short linker sequence (Alfano et al., 2004). Crystal structures of human La NTD have shown that the LAM contains five alpha helices and three antiparallel beta sheets that adopt a winged helix-turn-helix fold (Dong et al., 2004), while the RRM maintains a $\beta1\alpha1\beta2\beta3\alpha2\beta4$ fold, typical of other RRM-containing proteins. Briefly, the La module facilitates the binding of La to RNA polymerase III (RNAP III) transcripts via their common UUU-3'OH sequences (Teplova et al., 2006). The La module is also conserved in the LARP family (**Figure 1.1**), whose functions diverge from genuine La proteins, and are beyond the scope of this study.

In contrast, the C-terminal domains (CTDs) of La proteins tend to be less conserved and vary in length. In higher order eukaryotes, such as humans, La proteins contain a second RRM (RRM2) in the CTD that is predicted to have a role in targeting coding RNAs in the cytoplasm (Marrella et al., 2019). In La proteins lacking an RRM2, such as those found in both budding and fission yeast, the CTD facilitates additional RNA-binding and chaperone activity (Maraia et al., 2017). Various elements that control La's subcellular localization are also positioned in the CTD, including the nuclear retention element, nuclear localization signal, and short basic motif. These elements are found in differing combinations depending on the species and play key roles in the shuttling of La between the nucleus and cytoplasm where it interacts with different substrates (Fok et al., 2006). Due to this structural variation observed in the CTD, the size of La proteins can vary between 32 kDa in lower eukaryotes to 50 kDa in higher eukaryotes.

La proteins associate with several RNA targets and are involved in the regulation of their metabolism, and importantly, their folding. More detailed discussion of La's function and mechanisms of action is provided in section 1.3. However, La's function can generally be described as two-fold: simple 3' end protection of transcripts during maturation, and RNA chaperone activity.

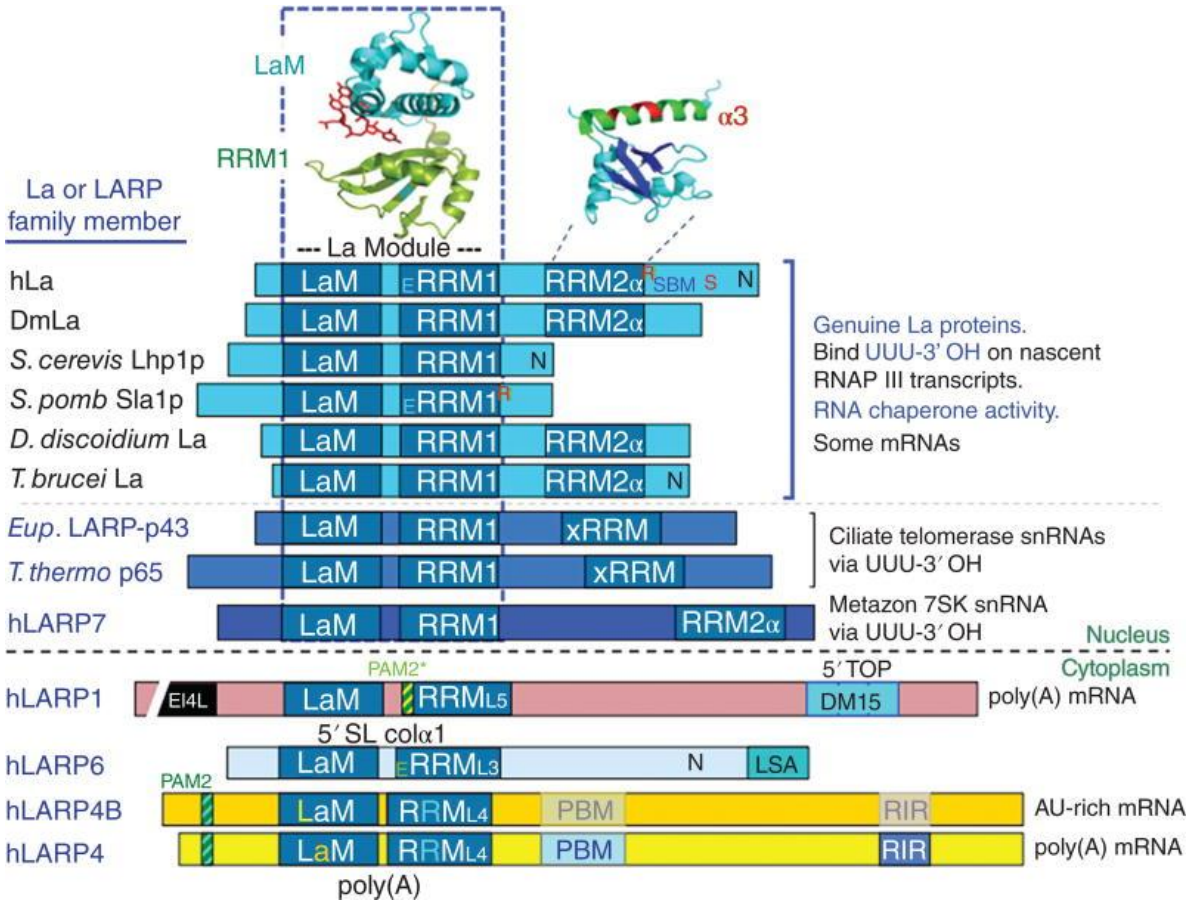

Figure 1.1: Schematic of the architecture of La protein homologs in various eukaryotes. The general architecture of La and La-related proteins (LARPs) in eukaryotes is conserved. Genuine La proteins (light blue) contain two adjacent RNA binding motifs in the N-terminal domain: the La motif (LAM) and RNA recognition motif (RRM1), that together form the highly conserved La module. The La module is also conserved in members of the LARP family. In higher eukaryotes, a second RRM (RRM2) is found in the C-terminal region. Figure adapted from (Maraia et al., 2017).

1.3 Pre-tRNA: La's preferred target

La is known to engage all nascent transcripts of RNAP III, including pre-5S rRNA, U6 snRNA, and 7SK RNA (Stefano, 1984). However, its best characterized substrates are precursor tRNAs (pre-tRNAs). As with many other types of RNAs, tRNAs are transcribed as larger

precursor molecules that require extensive processing. In contrast to genes transcribed by RNAPs I and II, the promotor elements for tRNA genes lie within the transcribed region. The key elements required for tRNA transcription are conserved sequences known as the A and B boxes that correspond to the defined D- and T-arms, respectively, of the natively folded tRNA (**Figure 1.2A**). The unique transcription termination process for RNAP III-transcribed genes drives their interaction with La. RNAP III terminates transcription following a tract of A residues encoded in the template DNA strand. The minimum length required for termination has been reported to be A_4 for humans and $A_{5\text{-}6}$ for yeast (Arimbasseri et al., 2013). During termination, the weak interactions between oligo(dA) in the template DNA strand and newly incorporated oligo(U) in the transcript act as a destabilizing signal, and the oligo(dT) tract of the non-template DNA strand promotes RNAP III pausing. Together, these promote the formation of the pretermination complex, and the release of the transcript (Arimbasseri et al., 2013). The nascent pre-tRNA is thus transcribed containing a 5' leader sequence averaging 10 bases, and a 3' trailer with a variable length of terminal uridylates that must both be processed prior to export from the nucleus (**Figure 1.2B**). Following nuclear export, any intron-containing species are appropriately spliced and charged with their cognate amino acid such that they can participate in translation.

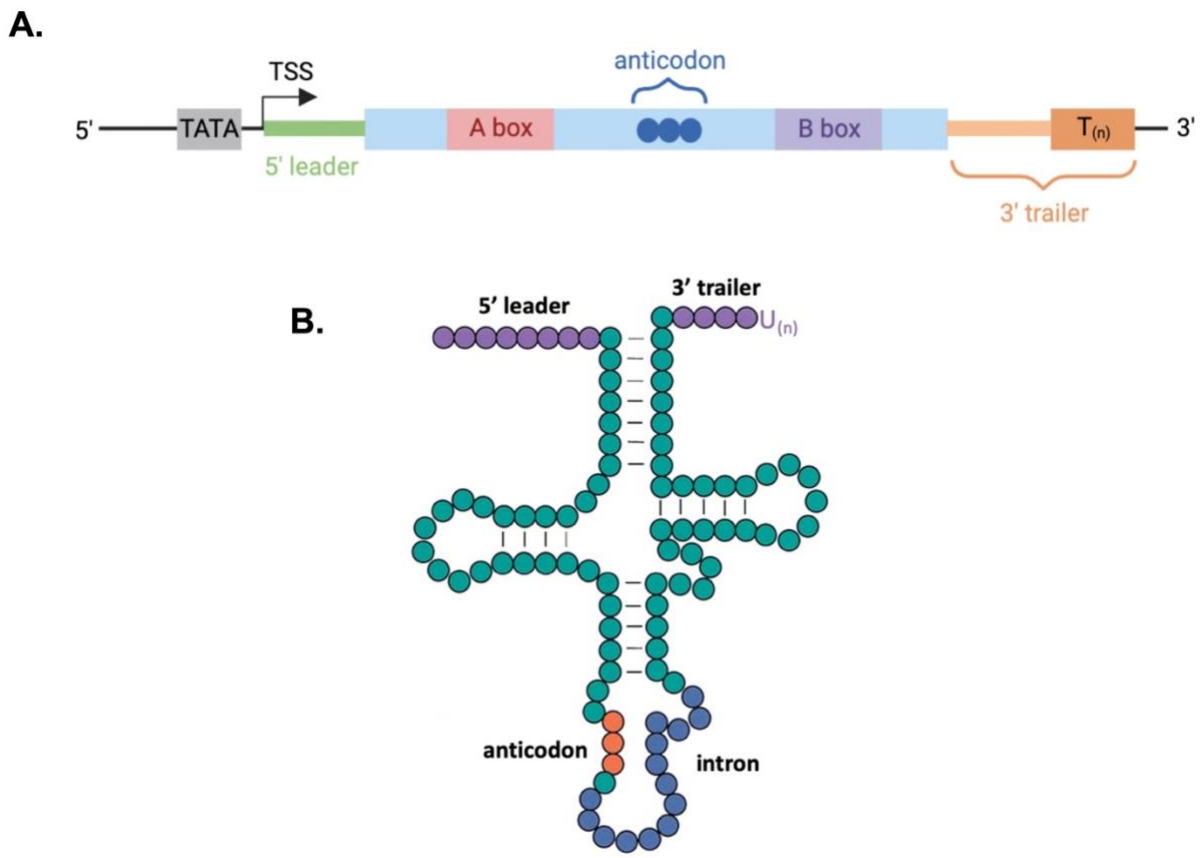

Figure 1.2: General architecture of tRNA genes and pre-tRNAs. (A): tRNA genes possess transcriptional regulatory elements within the transcribed region (A and B boxes) that correspond to conserved structures of the natively folded tRNA. The TATA box lies upstream of the transcription start site (TSS) and is occupied by an RNAP III transcription factor during transcription. Not drawn to scale. (B): tRNAs are transcribed as larger precursor molecules that must be processed prior to functioning in translation. Pre-tRNAs possess a short leader sequence on the 5' end, and a 3' trailer of variable length containing a stretch of uridylates that correspond to encoded thymidines involved in RNAP III termination. Some pre-tRNAs possess introns near the anticodon that must be spliced following their export from the nucleus. Figure A created in BioRender and Figure B adapted from (Hopper & Phizicky, 2003).

Natively folded mature tRNAs are often depicted in their clover leaf secondary structure. Complementarity between the 5' and 3' ends form the acceptor stem, which harbors the aminoacylation site on the 3' end. Other structured regions include the D-arm (so named

for the modified dihydrouridine base in the loop), anticodon arm, variable arm, and T-arm/TψC arm (so named for conserved thymidine, pseudouridine, and cytidine residues). Intramolecular interactions between the D- and T-arms facilitate tRNA folding into an L-shaped three-dimensional structure (Berg & Brandl, 2021) (**Figure 1.3**). Post-transcriptional modifications also heavily support tRNA structure. tRNAs are the most modified RNA species in the cell, with approximately 12% of bases bearing a modification (Berg & Brandl, 2021). While modifications in the anticodon arm support translational fidelity, those elsewhere on the tRNA (referred to as the tRNA 'body') promote interactions that drive native structure (Porat et al., 2021). As a result, tRNA modifying enzymes have been shown to function redundantly with RNA chaperones such as La with respect to promoting native fold (Vakiloroayaei et al., 2017).

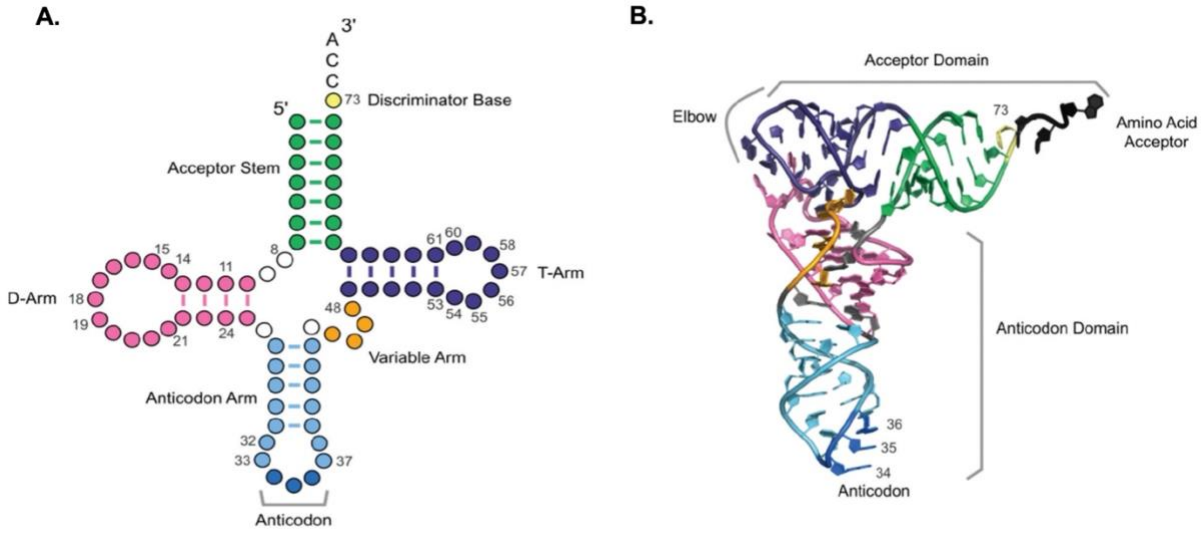

Figure 1.3: General secondary and tertiary structures of mature tRNAs. (A): Secondary structure resembles a clover leaf. Complementarity drives the formation of the various stems/arms depicted in differing colours. Natively folded mature tRNAs are aminoacylated on the 3' end of the acceptor stem (green). The A and B box regions of the tRNA gene correspond to the D- (pink) and T-arms (purple), respectively. The anticodon arm (light blue) contains the three-nucleotide anticodon that decodes complementary codons on mRNA. Some tRNAs possess an additional structured region called the variable arm (orange) that varies in length. (B): Intramolecular interactions drive the L-shaped tertiary structure. Colours for structured regions are consistent between the two diagrams. Figure adapted from (Berg & Brandl, 2021).

Co-crystal structures of the La module with a short RNA ligand terminating in UUU-3'OH have contributed to a detailed understanding of La's oligo(U)-dependent binding mode. These studies revealed that the three terminal uridylates of a substrate occupy a binding cleft formed by the LAM and RRM1 (**Figure 1.4**). Contacts are primarily mediated by hydrogen bonding and base stacking via conserved basic and aromatic residues of the LAM, with a 3' hydroxyl being a necessary determinant of binding (Kotik-Kogan et al., 2008; Teplova et al., 2006). Generally, La has higher affinity for pre-tRNAs with longer 3' uridylate tails. However, the minimum number of terminal uridylates required for La binding varies depending on the species, with at least U_3 being required for human La, and $U_{4\text{-}5}$ for yeast La (Huang et al., 2005; Stefano, 1984).

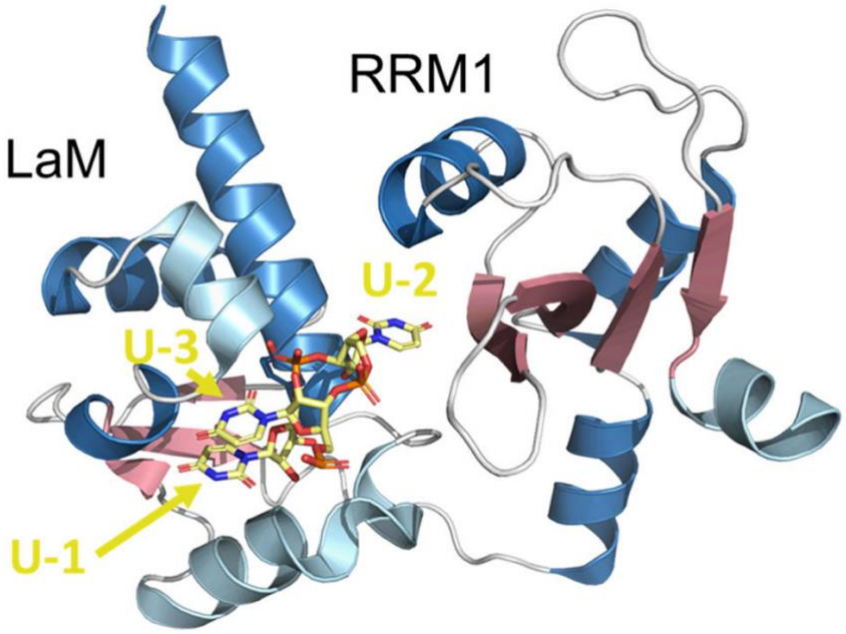

Figure 1.4: Three-dimensional rendering of the human La module interacting with a UUU-3'OH substrate. RNA shown in yellow; α-helices shown in blue; β-sheets shown in pink. The penultimate uridylate residue (U-2) is positioned within a binding cleft formed by the LaM and RRM1. Contacts to the other uridylates are made by the LaM. La chaperone activity is mediated by contacts between the RRM1 and body of the pre-tRNA (not shown). Figure adapted from (Kerkhofs et al., 2022).

This well-characterized interaction facilitates the simplest of La's two functions in the cell: 3' end protection from exoribonucleases during maturation. This interaction has been shown to drive the order of pre-tRNA processing in eukaryotic cells (Yoo & Wolin, 1997). Pre-tRNA processing can therefore occur via one of two pathways: the La-dependent processing pathway, or the La-independent processing pathway (**Figure 1.5**). Binding of La to the 3' uridylate trailer sequence imparts temporary protection from degradation by exoribonucleases such as Rex1p. Thus, following La binding to the uridylate tail, the 5' leader sequence is cleaved first by the endoribonuclease RNase P (Chamberlain et al., 1998). Following leader removal, the endoribonuclease RNase Z cleaves the 3' trailer sequence still bound by La (Yoo & Wolin, 1997). Following cleavage, La dissociates from the cleaved trailer and becomes available to bind other substrates. In contrast, in the absence of La, pre-tRNAs may undergo La-independent processing in which 3' trailer cleavage by Rex1p precedes 5' leader cleavage by RNase P.

Additional contact between an internal α-helix of the RRM1 and the penultimate uridine residue of the pre-tRNA leaves the RRM1 β-sheet exposed for contacts to the pre-tRNA body (Teplova et al., 2006). Mutations to basic and aromatic patches of the RRM1 were shown to not affect uridylate-dependent binding of pre-tRNAs, but rather resulted in defective chaperone activity *in vitro* and degraded pre-tRNAs *in vivo*. As a result, the RRM1 is suggested to possess chaperone function for the correct folding of tRNAs (Bayfield & Maraia, 2009; Huang et al., 2006). Finally, the disordered nature of La's CTD is thought to facilitate the transient binding with substrates required for repeated strand dissociation/binding for chaperone activity. While La's two binding modes can be thought of as distinct, it has been shown that intact La module (LAM + RRM1) has greater affinity for pre-tRNAs than either motif alone (Bayfield & Maraia,

2009). This cooperativity between La's two binding modes translates to cooperativity between La's functions during pre-tRNA maturation (**Figure 1.5**). In pre-tRNAs that are functionally impaired due to misfolding, La's chaperone activity promotes the acquisition of native structure and thus protects these species from degradation by the nuclear exosome.

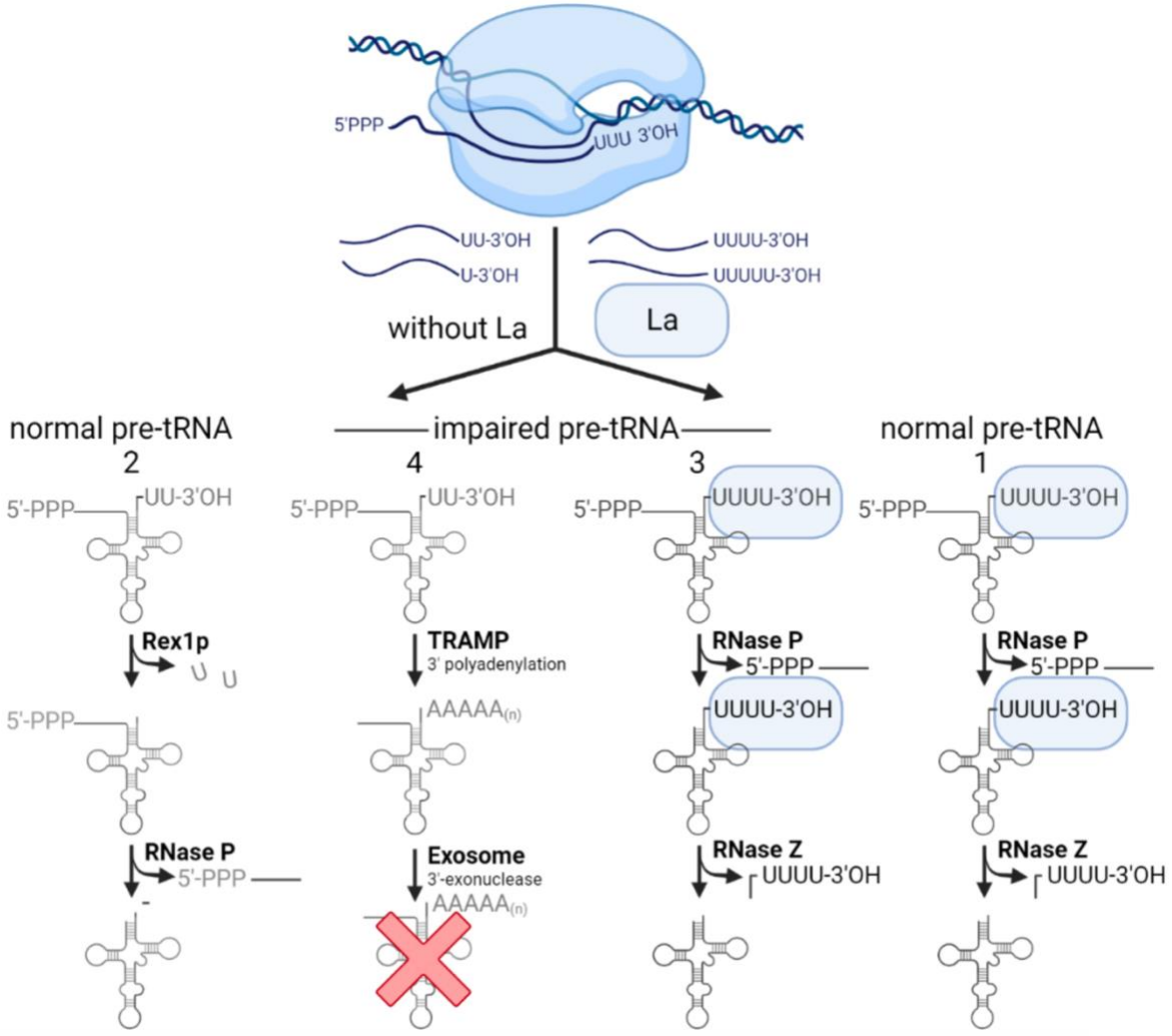

Figure 1.5: La influences the order of pre-tRNA processing. RNAP III transcribes pre-tRNAs containing a short 5' leader sequence and a 3' trailer with a variable number of terminal uridylates. Pre-tRNAs can undergo end-processing in a La-dependent or independent pathway. For natively folded pre-tRNAs, La binds the uridylate tail and temporarily protects the 3' end from degradation by exoribonucleases. The 5' leader is cleaved first by RNase P, followed by cleavage of the protected 3' end by RNase Z (pathway 1). In the absence of La, the 3' end of a normal pre-tRNA is exposed and degraded by the exoribonuclease Rex1p. The order of end-

processing is reversed in the absence of La (pathway 2). Structurally impaired pre-tRNAs benefit from La's chaperone activity during its binding for processing. La still offers temporary 3' end protection, but also assists with attaining native fold (pathway 3). In the absence of La, structurally impaired pre-tRNAs enter the nuclear surveillance pathway for quality control, where they are ultimately degraded by the nuclear exosome (pathway 4). Figure adapted from (Maraia & Lamichhane, 2011) and created by Kyra Kerkhofs in BioRender.

1.4 tRNA turnover

Mature tRNAs are highly stable, with half-lives ranging from hours to days (Huang & Hopper, 2016). In contrast, pre-tRNAs are more prone to misfolding and structural defects that ultimately lead to shorter-lived intermediates. Structural defects in pre-tRNAs may arise due to errors in transcription, nascent misfolding (kinetic RNA folding problem), hypomodification, and damage caused by environmental conditions. There is therefore a need for the quality control of tRNAs that possess processing, modification and folding defects. Interestingly, there exist two established tRNA quality control pathways: nuclear surveillance, and rapid tRNA decay (RTD).

The nuclear surveillance pathway is generally classified by the 3' to 5' exonucleolytic degradation of misfolded pre-tRNAs by the nuclear exosome. In this pathway, structurally aberrant pre-tRNAs are polyadenylated at the 3' end by the TRAMP (*Trf4/5*, *Air1/2*, *Mtr4*, polyadenylation) complex. Although poly(A) tails on mRNAs impart protection and stability, the shorter polyadenylation of defective pre-tRNAs promotes 3' to 5' degradation by nuclear exosome exonucleases such as Rrp6. (Kadaba et al., 2004, 2006). Interestingly, a large-scale study on catalytic mutants within the nuclear exosome revealed that as many as 50% of pre-tRNAs may be degraded via the nuclear surveillance pathway (Gudipati et al., 2012). In contrast,

RTD is driven by a lack of stabilizing modifications. In this pathway, specific hypomodified mature tRNAs are degraded in a 5' to 3' manner by the exonucleases Xrn1 or Rat1 (Chernyakov et al., 2008).

As illustrated in **Figure 1.5**, the nuclear surveillance pathway is closely linked to pre-tRNA maturation, and by association, La. In addition to chaperone activity, La blocks access to the 3' end of pre-tRNAs by the nuclear exosome (Huang et al., 2006). tRNA turnover pathways like nuclear surveillance support cell function by eliminating misfolded, functionally impaired tRNAs. Due to the abundance of tRNAs in the cell, if tRNA turnover pathways were the cell's only strategy to manage aberrant tRNAs, it is conceivable that the system would be overwhelmed with circulating impaired tRNAs, leading to errors in translation. This notion points to the importance of the La protein as a key factor that helps drive native tRNA structure and reduce degradation by surveillance.

1.5 The effects of cellular stress on tRNAs

Changes in a cell's environment affect many independent and overlapping cellular processes. Cells respond to changes in environment mainly via conserved signaling cascades that often result in the up- or down-regulation of genes involved in cell cycle progression/arrest or a particular response pathway, with extreme stress often resulting in cell death.

As previously highlighted, the three-dimensional structure of RNA is highly sensitive to perturbations that may be caused by a multitude of factors. While many of these perturbations occur in an unprovoked nature, it is widely understood that various environmental stresses

negatively impact overall RNA stability. Oxidative stress is one of the most widely studied stresses on eukaryotic cells. Oxidative stress is induced by the formation of free radicals: highly reactive entities with unpaired electrons. Although free radicals play physiological roles in the cell, their high reactivity allows them to participate in unwanted side reactions that result in cellular damage (Kong & Lin, 2011). The hydroxyl free radical (denoted $OH^{\bullet}$) is formed via the degradation of H_2O_2 in the presence of Fe^{2+} and is responsible for most oxidative damage to biological molecules in the cell (Kong & Lin, 2011). Several lines of evidence point to the higher vulnerability of RNA to oxidative damage versus DNA and even other biological macromolecules. Using *in situ* immunohistochemistry in neurodegenerative disease tissues, it has been shown that most oxidized nucleosides in cells belong to RNA rather than nuclear or mitochondrial DNA (Nunomura et al., 1999, 2002). $OH^{\bullet}$ radicals produced in the vicinity of RNA can easily modify bases due to their high reactivity and difficulty diffusing from their site of formation (Kong & Lin, 2011). The most common oxidative modification to RNA is the formation of 8-hydroxyguanosine (8-OHG). Although oxidative modifications to mRNA have been linked to ribosome stalling (Shan et al., 2007), in some instances, 8-OHG in the second codon position has been shown to base pair with adenosine in tRNA anticodons, leading to potential amino acid misincorporation during protein synthesis (Tanaka & Chock, 2021). Currently, there are no known repair mechanisms for oxidized RNAs (Ørom et al., 2020; Li et al., 2006).

Perhaps the most basic environmental stress that affects RNA structural dynamics is heat stress. The hydrogen bonds that mediate secondary and tertiary RNA structure may break (or melt) in response to heat, ultimately resulting in RNA unfolding. In addition, higher temperatures may also irreversibly hydrolyze RNA more readily than DNA due to interaction

between the 2'-OH found only in RNA and adjacent phosphate group (Becskei & Rahaman, 2022). Overall, structured ncRNAs are highly susceptible to thermal denaturation and degradation. In contrast, nutrient starvation is a cellular stress that has less obvious and defined impacts on RNA structure. However, one group recently found through northern blotting that bacterial tRNAs are rapidly degraded during amino acid starvation (Svenningsen et al., 2017). Although not yet proven, it is possible that this response is conserved for eukaryotic tRNAs. Furthermore, if tRNAs are degraded in a 3' to 5' manner during amino acid starvation, it is also possible that La may play a direct role in their metabolism during stress.

Recent works in the budding yeast *Saccharomyces cerevisiae* have shown that environmental stresses influence many steps of tRNA biology, especially processing, modification, subcellular dynamics, and fragmentation (**Figure 1.6**). These studies demonstrate that cellular stresses lead to the accumulation of aberrant tRNAs, often in a tRNA-specific manner, shifting the equilibrium away from native tRNA structure and function. For example, northern blotting and RNA sequencing experiments have shown that heat stress and changes in nutrient source inhibit the 3' end processing of tRNA Tyr and tRNA Ile^{UAU} (Foretek et al., 2016). Additionally, heat and oxidative stress have been shown to reprogram the tRNA modification landscape, ultimately leading to alterations in tRNA structural stability (Agris et al., 2007; Yarian et al., 2002). For example, thiolation of uridine bases (S2U) is a common modification found in the anticodon loop of tRNAs known to impart increased translational fidelity. When found in the wobble position of the anticodon, S2U facilitates Watson-Crick base-pairing with adenosine and restricts wobble base-pairing with guanosine (Agris et al., 2007; Yarian et al., 2002). Additionally, S2U modification in the anticodon loop serves as a recognition element for amino

acid tRNA synthetases, the enzymes that aminoacylate tRNAs. Oxidative environments have been shown to dethiolate RNA (Chan et al., 2010). Therefore, alterations to the tRNA modification landscape caused by oxidative environments may decrease translational fidelity by disrupting codon-anticodon interaction and promoting non-cognate aminoacylation. Furthermore, tRNA trafficking in the cell is sensitive to changes in nutrient availability. tRNA retrograde nuclear import is constitutive, and so tRNA subcellular localization is mainly controlled at the level of re-export to the cytoplasm (Murthi et al., 2010). Various tRNA isoacceptors have been shown to accumulate in the nucleus following nutrient deprivation (Shaheen & Hopper, 2005; Whitney et al., 2007). Finally, oxidative stress has also been shown to result in the enzymatic cleavage of mature tRNAs in the anticodon loop, leading to the cytoplasmic accumulation of tRNA halves (Thompson et al., 2008). Although the functions of tRNA halves are not well-characterized, they are thought to have various regulatory roles in the cell (Huang & Hopper, 2016).

Overall, there exists an abundance of crosstalk between cellular stresses and their effects on tRNA biology. While many facets of tRNA biology are conserved, exploring tRNA response to stress, especially in other organisms, will further understanding of the roles of tRNAs beyond translation, and provide additional insight into how cells respond to their environment. Furthermore, any possible crosstalk between La function, tRNA processing, and changes in tRNA processing during stress has not previously been explored.

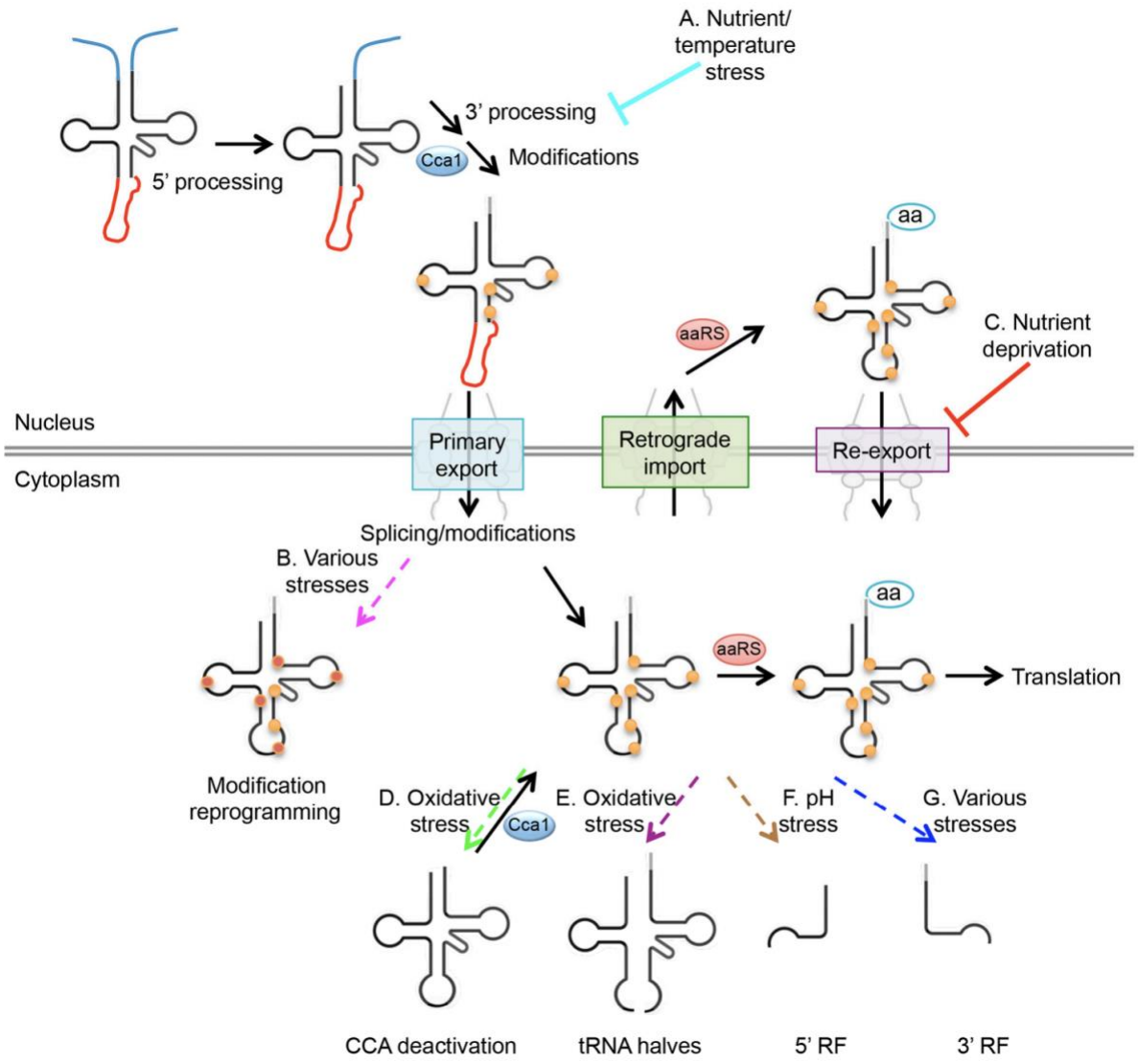

Figure 1.6: Stress-induced regulation of tRNAs is multifaceted. Black arrows represent canonical tRNA maturation and function. Cellular stresses impact all steps along the canonical tRNA pathway. (A): 3' end processing is inhibited by changes in nutrient sources and heat stress, leading to an accumulation of nuclear pre-tRNAs with extended 3' ends. (B): Multiple stresses reprogram the modification landscape of tRNAs, leading to changes in structural stability. (C): Nutrient starvation stress inhibits re-export of tRNAs into the cytoplasm, leading to the nuclear accumulation of various tRNA species. (D-G): Various stresses, especially oxidative stress, lead to the endonucleolytic cleavage of tRNAs at various sites, resulting in the accumulation of functional tRNA-derived halves and fragments. Figure adapted from (Huang & Hopper, 2016).

1.6 Thesis rationale and proposal

La's role in pre-tRNA processing is well-characterized. However, like other RNA chaperone proteins, detailed mechanisms surrounding its chaperone activity are yet to be elucidated. A key question in the study of RNA chaperone proteins is whether they discriminate among potential RNA substrates based on fold for chaperone activity. Several studies have shown that many RNA chaperone proteins do not discriminate between natively folded and misfolded RNA substrates, and rather, promiscuously engage substrates regardless of fold status (Huang et al., 2006; Keffer-Wilkes et al., 2016; Tijerina et al., 2006). However, this model of RNA chaperone activity benefits misfolded RNAs by rescuing them from surveillance at the expense of processing efficiency for correctly folded RNAs. Since La is limiting in the cell relative to pre-tRNAs and other RNAP III transcripts (Huang et al., 2005), discrimination of RNA substrates based on fold would be energetically favourable for the cell.

Previous work in our lab concluded that the fission yeast *Schizosaccharomyces pombe* La protein homolog (Sla1p) also does not discriminate between natively folded and misfolded pre-tRNAs for chaperone activity (Vakiloroayaei et al., 2017). However, a caveat to this study was that it was limited in scope to pre-tRNAs that were modifiable by a stabilizing post-transcriptional modification by the methyltransferase Trm1p. Its scope was also limited by low-throughput techniques that rely on probe functionality such as northern blotting and qRT-PCR. This thesis expands on this work by both exploring potential substrate discrimination by Sla1p across all pre-tRNAs, as well as in the context of potentially misfolded or misprocessed tRNAs that may occur under conditions of cellular stress. Central to this work was the generation of a custom polyclonal antibody against Sla1p. This pioneering method in our lab allowed for higher

specificity in immunodetection assays to avoid confounding issues that arise due to conducting these experiments in protein-tagged yeast strains. Using the custom α-Sla1p antibody, we utilized a workflow whereby native Sla1p-RNA complexes were immunoprecipitated from variably stressed *S. pombe* cells, and isolated Sla1p-bound RNAs were identified and quantified via RNA sequencing. As such, the scope of the investigation was broadened by inducing RNA misfolding in more than one way, as well as by using a high-throughput, unbiased method to query Sla1p's entire RNA interactome.

The first step of traditional RNA sequencing is the synthesis of complementary DNA (cDNA) from an RNA template by reverse transcriptase enzymes. This step proves to be challenging for highly structured and modified RNAs such as tRNAs. Secondary structure causes inefficient adapter ligation, and modifications cause reverse transcriptase stalling, progressively limiting the generation of full-length cDNA reads (Arimbasseri et al., 2015). Recently, advances have been made to overcome these limitations, such as pre-treating tRNAs with enzymes that remove blocking modifications (Cozen et al., 2015; Zheng et al., 2015). Additionally, a method termed 'tRNA-HydroSeq' employs limited alkaline hydrolysis to produce shorter tRNA fragments that have less potential to form secondary structures and possess fewer modifications (Arimbasseri et al., 2015; Karaca et al., 2014). Notably, tRNA-HydroSeq captures modification information through misincorporation of bases by reverse transcriptase at some modified bases (Arimbasseri et al., 2015). While this can be informative for some applications, the most recently developed, and gold standard method for tRNA sequencing involves the use of the highly processive and structure-tolerant thermostable group II intron reverse transcriptase (TGIRT) (Nottingham et al., 2016; Qin et al., 2016). This sequencing method

(TGIRT-seq) thus permits the full-length sequencing of highly structured and modified tRNAs (Boivin et al., 2020).

Overall, this project aimed to gain an unbiased view of Sla1p's RNA interactome under both normal and stress conditions. We hypothesized that Sla1p preferentially engages certain pre-tRNA targets for chaperone intervention under various cellular stresses due to increased target misfolding. Using TGIRT-seq as a primary method, this project had three goals:

1. Characterize Sla1p's RNA targets into stress-specific cohorts.
2. Identify any structure and/or sequence motifs that may explain increased or decreased interaction with Sla1p during stress.
3. Investigate stress-specific alterations to Sla1p-dependent pre-tRNA processing.

To achieve the first goal, we looked for changes in Sla1p's RNA interactome under various cellular stresses that may impact RNA folding, stability, or maturation in comparison to normally grown cells. Specifically, we chose to implement oxidative stress via H_2O_2, heat stress, and nutrient starvation via growth through stationary phase. Should our hypothesis be correct, completion of the second objective may provide insight into why Sla1p may engage certain RNA substrates over others during stress. Given the established impacts of environmental stress on tRNA processing in other organisms, our third goal may lead to novel insights with respect to tRNA processing in *S. pombe*.

It is hoped that this work will provide progress towards identifying the ambiguous mechanisms behind La's chaperone activity. On a clinical scale, the human La protein has been shown to be implicated in many cancers including ovarian and lung (Huang & Tang, 2020;

Kaliatsi et al., 2020). La is overexpressed in various malignant tumors and is thought to be related to tumor cell proliferation, invasion, and metastasis, and can therefore serve as a drug target during cancer therapy (Huang & Tang, 2020). However, details of La's involvement in cancer progression are not fully understood. Although this research project will not directly shed light onto this subject, new knowledge on substrate discrimination by La proteins may be helpful in further understanding La's role in cancer.

CHAPTER 2: MATERIALS AND METHODS

2.1 Generation of custom α-Sla1p polyclonal antibody

2.1.1 Plasmid Isolation

XL1-Gold competent *E. coli* cells containing the pET23a expression plasmid with inserted *sla1* bearing a C-terminal 6x-His tag were grown on LB agar plates containing 0.1 mg/mL ampicillin for selection. Selected colonies were grown at 37°C overnight in 5 mL LB media containing 0.1 mg/mL ampicillin. Plasmid DNA was isolated using the GeneJET plasmid miniprep kit (Invitrogen cat. #K0502) according to the manufacturer's instructions.

2.1.2 Bacterial transformation and induction of Sla1p expression

Extracted plasmid DNA was transformed into competent BL21 *E. coli* cells for inducible expression of Sla1p-6x-His. A 1 in 100 dilution of plasmid DNA was prepared and 2 μL was added to 25 μL of thawed BL21 cells and incubated on ice for 20 minutes. Following incubation, the cells were heat shocked in a 37°C water bath for 90 seconds and were allowed to rest on ice for 2 minutes. 200 μL of LB media was added to the transformed cells, followed by recovery at 37°C, shaking at 200 rpm for 1 hour. The transformed cell mixture was plated on LB agar plates containing 0.1 mg/mL ampicillin, using sterile glass beads to spread. Plates were left to grow overnight at 37°C.

A 50 mL overnight culture of transformed BL21 cells was made in LB media containing 0.1 mg/mL ampicillin and grown to saturation. The entirety of the overnight culture was then used to seed into 2 L of LB media containing 0.1 mg/mL ampicillin and was grown at 37°C with

shaking at 200 rpm until OD_{600nm} = 0.6-0.8 (mid-log phase). Protein expression was induced with IPTG (final = 1 mM) for 3 hours at 37°C.

2.1.3 Purification of Sla1p by Ni^{2+} affinity chromatography

Following induction, cells were harvested by pelleting at 4°C and 7500 x g for 10 minutes. Pellets were resuspended in 50 mL of Pellet Eluting Buffer (50 mM Tris-HCl pH 7.4, 100 mM NaCl) and re-pelleted at 4°C and 5700 x g for 12 minutes.

To begin cell lysis, pellets were resuspended in 10 mL Lysis Buffer (50 mM Tris-HCl pH 7.6, 500 mM NaCl, 0.05% NP40, 20 mM imidazole, 5 mM β-Mercaptoethanol) by vortexing on and off ice. Following resuspension, 100 μL each of Protease Inhibitor Cocktail (PIC) (ThermoFisher) and 100 mM phenylmethylsulfonyl fluoride (PMSF) were added for protease inhibition. Cells were subsequently sonicated on ice in 15 second on/off intervals for 12 minutes at 0.05 W. To remove cellular debris, sonicated samples were then spun at 4°C and 20,000 x g for 40 minutes, and the supernatant (cell lysate) was transferred to a 15 mL conical tube.

To begin purification, a Ni^{2+}-His trap column (Sigma Millipore) was washed with 5 mL of ddH_2O and equilibrated with 5 mL of Lysis Buffer using a sterile syringe. 10 mL of cell lysate was passed through the column, and flow-through was collected in a 15 mL conical tube. The column was then washed five times with 5 mL Wash Buffer (50 mM Tris-HCl pH 7.6, 500 mM NaCl, 20 mM imidazole, 5 mM β-Mercaptoethanol) for each wash. Flow-through from each wash was collected in separate 15 mL conical tubes. Sla1p-6x-His was eluted from the column

with 5 mL Elution Buffer (50 mM Tris-HCl pH 7.6, 500 mM NaCl, 300 mM imidazole, 5 mM β-Mercaptoethanol, 1 mM EDTA) and collected in a 15 mL conical tube.

Eluted Sla1p was concentrated in a 10 kDa concentrator tube via centrifugation at 4°C and 4200 x g until a volume of 500 μL was reached. To exchange the buffer for storage, two rounds of buffer exchange were performed as follows: 4 mL of PBS was added to the concentrator and spun at 4°C and 4200 x g for 35 minutes. Concentrated and buffer-exchanged protein was stored at -80°C with 50% glycerol.

2.1.4 Quantification of Sla1p concentration

Quantification of purified protein was conducted by comparison to bovine serum albumin (BSA) standards after separation by SDS-PAGE. Four samples of Sla1p were prepared using 0.05 μL, 0.1 μL, 0.25 μL, and 0.5 μL of purified Sla1p, and diluting with ddH_2O to a final volume of 12 μL. Similarly, four 12 μL samples of BSA were prepared containing 1 μg, 2 μg, 4 μg, and 8 μg of BSA. Each sample was brought to 15 μL by adding 3 μL of 5X Laemmli Sample Buffer (250 mM Tris-HCl pH 6.8, 5% SDS, 30% glycerol, 0.12% bromophenol blue, 10% β-Mercaptoethanol), and heated at 95°C for 10 minutes. Samples were resolved on a 10% SDS-PAGE gel at 100 V for 80 minutes. Protein was visualized by staining with Coomassie Brilliant Blue Dye (50% methanol, 10% glacial acetic acid, 0.1% Coomassie Blue) followed by de-staining (40% methanol, 10% glacial acetic acid).

2.1.5 Raising rabbit polyclonal antibody

6.7 mg of purified Sla1p was shipped to Pierce Custom Services (ThermoFisher Scientific) for immunization into two rabbit models and affinity purification of α-Sla1p polyclonal

antibodies. Their "2 rabbit, 90 day" protocol was followed, consisting of 3 antigen boosts and 4 bleeds per animal.

2.2 Custom antibody validation and optimization

In order to validate the efficacy of the custom anti-Sla1p polyclonal antibody, lysates from various *S. pombe* strains were assessed for Sla1p presence by western blotting using the custom α-Sla1p antibody as primary antibody. Optimization of primary antibody concentration followed.

2.2.1 Plasmid isolation

XL1-Gold competent *E. coli* cells containing the pRep4 expression plasmid – either an empty vector or expressing the *sla1* gene were grown on LB agar plates containing 0.1 mg/mL ampicillin for selection. Isolation of plasmid DNA was conducted as described in section 2.1.1.

2.2.2 Yeast transformation

pRep4 (empty) and pRep4-*sla1* were transformed into wild-type or Δ*sla1 S. pombe* strains. Wild-type and Δ*sla1* yeast strains were each grown at 32°C in 20 mL YES media (5 g/L yeast extract, 225 mg/L each adenine, histidine, leucine, lysine, uracil, 15% dextrose) to mid-log phase. Cells were pelleted at 4°C and 1900 x g for 10 minutes and resuspended in 40 mL of sterile H_2O. Resuspended cells were pelleted again at the previous conditions. New pellets were resuspended in 200 μL of chilled LiAc-TE buffer (1X LiAc, 10 mM Tris pH 8, 1 mM EDTA), and 100 ug salmon sperm DNA (Invitrogen) was added. 100 μL of each cell mixture was added to 2 μL of each purified plasmid (pRep4 or pRep4-*sla1*). To each transformation mixture, 700 μL of LiAc-

TE-PEG Buffer (1X LiAc, 10 mM Tris pH 8, 1 mM EDTA, 40% PEG) was added and vortexed. Cells were subsequently heat shocked at 42°C for 15 minutes and pelleted at 5500 x g for 1 minute. The supernatant was aspirated, and the transformed pelleted cells were resuspended in 200 μL of sterile ddH_2O. The entirety of the 200 μL were plated on Edinburgh minimal media lacking uracil (EMM-Ura) agar plates (11.8 g/L EMM-glucose base, 225 mg/L each of adenine, histidine leucine, lysine, 10% dextrose) using sterile glass beads to spread, and were left to grow at 32°C.

2.2.3 Protein extraction and western blotting

Total cell lysates of various untransformed yeast strains and transformed strains (see section 2.2.2) were prepared for the purpose of detecting either endogenous or recombinant Sla1p with the custom polyclonal anti-Sla1p antibody via western blotting. 30 mL cultures of each strain or transformation were grown at 32°C in appropriate media (YES for untransformed strains, and EMM-Ura for transformed strains) until mid-log phase. Cells were pelleted at 4°C and 1100 x g for 5 minutes and the pellets were resuspended in 1 mL of ddH_2O and re-pelleted at the previous conditions. The new pellets were resuspended in 100 μL of chilled NET-2 Lysis Buffer (50 mM Tris pH 7.5, 150 mM NaCl, 0.05% NP40, 0.1 mM PMSF), and approximately 150 μL of sterile 0.5 mm glass beads were added to each cell mixture for lysis. In a cold room, cells were lysed using a Bead Beater (BioSpec), cycling between 20 seconds of beating followed by 2 minutes of rest on ice, until 1 minute of beating was achieved. Following lysis, an additional 100 μL of chilled NET-2 Lysis Buffer was added to each sample, and debris was sedimented by centrifugation at 4°C and 20,000 x g for 5 minutes. The supernatants were transferred to clean microfuge tubes and an additional 100 μL of chilled NET-2 Lysis Buffer was added to the pellets

and beads. To ensure the collection of as much lysate as possible, the mixtures containing the beads were centrifuged again as described above and the lysates were collected and added to their respective tubes. Each microfuge tube was then centrifuged at 4°C and maximum speed for 35 minutes to pellet any glass beads that may have been collected along with the supernatant. Each lysate was then again transferred to a new microfuge tube.

12 μL of each lysate was mixed with 3 μL of 5X Laemmli Sample buffer to a final 1X dilution. Samples were heated at 95°C for 10 minutes prior to electrophoresis on a 10% denaturing SDS polyacrylamide gel. The samples were resolved at 100 V for 80 minutes and transferred to a nitrocellulose membrane (Novex, ThermoFisher Scientific) at 50 V for 90 minutes. Following transfer, the membrane was blocked with Blocking Buffer (5% skim milk powder, 1X TBS, 0.1% Tween-20) for 1 hour. The membrane was then incubated in [1:2000] primary custom antibody in TBST (1X TBS, 0.1% Tween-20) for 1 hour, and washed three times in 10-minute intervals with TBST. Subsequent western blot attempts for primary antibody dilution optimization used [1:2000] and [1:10,000] dilutions of custom α-Sla1p. Following washing, the membrane was incubated in [1:5000] HRP-conjugated α-rabbit IgG secondary antibody (NEB cat. #7074S) for 1 hour and washed as above. Signal was visualized by incubation in ECL Western Blotting Substrate (ThermoFisher Scientific) for 2 minutes and imaged using a MicroChemi imager (DNR Bio-Imaging Systems).

2.3 Preparation of TGIRT RNA-seq samples and quality assessment

2.3.1 Induction of cellular stresses on *S. pombe* cells

Three cellular stresses predicted to negatively impact pre-tRNA structure *in vivo* were applied to wild-type *S. pombe* cells to ascertain whether Sla1p discriminates between a misfolded and natively folded substrate. The stresses chosen include oxidative stress via H_2O_2, heat stress, and stationary phase stress (a form of nutrient starvation).

Twelve 1 L cultures of wild-type *S. pombe* cells were grown in YES media at 32°C (three stresses plus unstressed control, each in biological triplicate). All stresses were applied when the cells reached mid-log phase except stationary phase stress, which were grown until $OD_{600nm} \geq 2$. Oxidative stress was induced by adding H_2O_2 to the liquid cultures to a final concentration of 1 mM while shaking at 32°C for 30 minutes. Heat stress was induced by transferring cells to 42°C while shaking for 15 minutes. Once all stresses were applied, RNP complexes were crosslinked by adding formaldehyde (final = 0.2%) to the liquid cultures and shaking at room temperature for 20 minutes. The crosslinking reaction was quenched with glycine (final = 200 mM) while shaking at room temperature for 5 minutes.

Cells were harvested by pelleting at 4°C and 3300 x g for 10 minutes, and the pellets were washed with 45 mL sterile ddH_2O. The cells were then pelleted again at the previous conditions. Washed pellets were resuspended in 5 mL of Resuspension Buffer (1.2% PVP40, 20 mM HEPES pH 7.4, 1% PIC, 1 mM PMSF, 1 mM DTT) and re-pelleted at the previous conditions. Yeast powder (grindate) was obtained from the pellets using a technique described by (Oeffinger et al., 2007), summarized below in **Figure 2.1**. Dry pellets were flash-frozen via

injection into liquid nitrogen using sterile syringes, and subsequently broken in the solid phase using a mortar and pestle to obtain cell grindate.

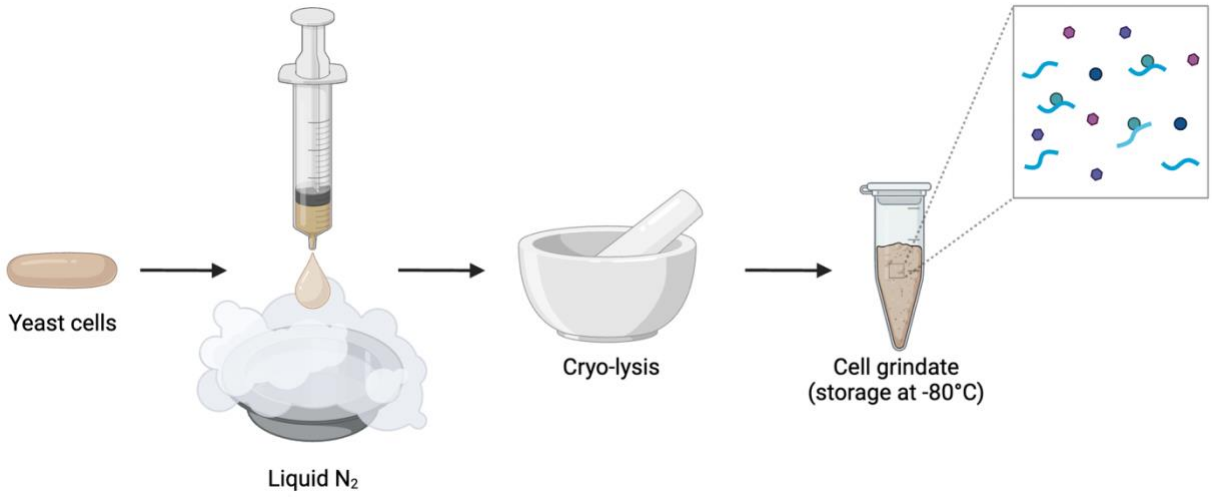

Figure 2.1: Schematic outlining the protocol for obtaining yeast cell grindate from a harvested pellet. Yeast cells are flash-frozen by injection into liquid nitrogen and ground into a powder using either a mortar and pestle or planetary ball mill. Figure adapted from (Oeffinger et al., 2007) and created in BioRender.

2.3.2 RNA immunoprecipitation (RIP) and RNA extraction

For all cellular conditions and replicates, Sla1p was immunoprecipitated using the custom α-Sla1p antibody conjugated to Protein-A magnetic Dynabeads (ThermoFisher Scientific). Non-immune rabbit IgG (Cell Signaling Technology cat. #3678S) was similarly conjugated to beads and used in parallel for IPs as a negative control.

30 μg of antibody (AB2597 or rabbit IgG) was added to PBS + 0.1% Tween-20 to a final volume of 100 μL and conjugated to beads via rotation at 4°C for 40 minutes. Rabbit IgG-conjugated beads were similarly prepared for pre-clearing lysates using half the quantity of beads and antibody used for IP. Following conjugation, beads were washed twice with 500 μL of PBS + 0.1% Tween-20, and three times with 1 mL of 1X RNP Buffer (20 mM HEPES pH 7.4, 110

mM KOAc, 100 mM NaCl, 1 mM PMSF, 1X PIC (ThermoFisher Scientific), 0.1% Tween-20, 0.5% Triton X-100, 0.2 μL/mL RNase inhibitor (Invitrogen)). Cell lysates were prepared by dissolving 0.4 g of grindate in 3.6 mL of 1X RNP Buffer. Cells were pelleted at 4°C and 1200 x g for 10 minutes. The supernatant (cell lysate) was pre-cleared with rabbit IgG-coupled beads by rotating at 4°C for 40 minutes. 24 μL and 180 μL of pre-cleared lysate was retained for downstream western blot validation and input RNA extraction, respectively. The remainder of the cell lysates were divided equally between AB2597-conjugated beads and rabbit IgG-conjugated beads and rotated at 4°C for 2 hours for immunoprecipitation.

Following incubation, the remainder of the lysates (flow-throughs) were transferred to sterile microfuge tubes. Beads bound with Sla1p RNP complexes or rabbit-IgG were washed three times with 1 mL of 1X RNP Buffer and eluted in 400 μL of 1X RNP Buffer. Elutions were rotated again at 4°C for 5 minutes. 40 μL of the elutions (including beads) was removed into new tubes, buffer was removed via magnetization, and the beads were resuspended in 30 μL of 5X Laemmli Sample Buffer for downstream validation via western blot.

To the remaining input lysates and 360 μL of elution, RNAse-free SDS (final = 0.125%), and Proteinase K (final = 1 μg/μL) were added, and the samples were heated at 37°C for 1 hour. Reverse crosslinking was performed by subsequently heating the samples at 65°C for 1 hour. Following reverse crosslinking, an equal volume of phenol:chloroform:isoamyl alcohol (25:24:1) was added to each sample and vortexed until thoroughly mixed. The aqueous layer obtained from centrifugation at 14,000 x g for 10 minutes was transferred to a sterile microfuge tube. To each aqueous sample, 2 μL of GlycoBlue coprecipitant (Invitrogen cat. #AM9515), 10% of the

isolated sample volume of 3M NaOAc pH 5.2, and 2.5X the isolated sample volume of ice-cold 100% ethanol was added. RNA was left to precipitate overnight at -80°C.

2.3.3 Total RNA extraction from wild-type and Δ*sla1* cells

In order to assess any changes in global RNA levels in the absence of Sla1p, total RNA was extracted from three biological replicates of wild-type and Δ*sla1 S. pombe* cells using the hot phenol method.

Wild-type and Δ*sla1* cultures were grown to mid-log phase in 25 mL of YES media at 32°C. Cultures were pelleted at 4°C and 1900 x g for 10 minutes and pellets were washed with 25 mL of sterile ddH_2O, then re-pelleted at the previous conditions. Pellets were resuspended in 500 μL of nuclease-free H_2O and transferred to sterile microfuge tubes. Cells were re-pelleted at the previous conditions and pellets were subsequently washed with 250 μL of complete RNA Extraction Buffer A (50 mM NaOAc pH 5.2, 10 mM EDTA pH 8.0, 1% SDS). 750 μL of warm Buffer A-saturated acid phenol was then added to each sample. The samples were vortexed to resuspend the pellet in the buffers and were incubated at 65°C for 4 minutes, vortexing occasionally. The samples were subsequently centrifuged at maximum speed for 3 minutes and the aqueous layer was transferred to a new sterile microfuge tube. An additional 250 μL of complete RNA Extraction Buffer A was added to the initial tubes with cells and a second round of RNA extraction was performed as described above, adding the aqueous layer to the corresponding tubes and discarding the phenol layer. Phenol-chloroform RNA extraction and precipitation was performed on the aqueous samples as described in section 2.3.2.

2.3.4 RNA size exclusion and precipitation

Precipitated input RNA, Sla1p-associated RNA, and total RNA from wild-type and Δ*sla1* cells (see sections 2.3.2 and 2.3.3) were pelleted at 4°C and 14,000 x g for 10 minutes. Pellets were washed with 500 μL of ice-cold RNase-free 70% ethanol and re-pelleted at the previous conditions. Pellets were air-dried and resuspended in 7 μL of nuclease-free H_2O and 7 μL 2X formamide dye (80% deionized formamide, 10 mM EDTA, 0.06% bromophenol blue, 0.06% xylene cyanol). RNA samples were heated at 95°C for 5 minutes and snap-cooled on ice prior to separation on a 10% denaturing urea gel (8 M urea, 10% acrylamide, 1X TBE) at 100 V until the xylene cyanol dye front reached the bottom of the gel. Following staining with EtBr in 1X TBE (1 μL/5 mL), the gel was visualized under UV light and RNAs were size selected (20-150 nucleotides) by cutting each lane between the bands corresponding to the 5S and 5.8S rRNAs and retaining the lower halves in microfuge tubes. RNA was eluted from the gel pieces by overnight rotation at 4°C in 150 mM NaOAc pH 5.2 and 50% phenol:chloroform:isoamylalcohol (25:24:1). The aqueous layer obtained by centrifugation at 4°C and 20,000 x g for 10 minutes was precipitated as described in section 2.3.3.

Precipitated RNA for all samples were pelleted, washed, and air-dried as described above. Pellets were resuspended in 20 μL nuclease-free H_2O and shipped to our collaborators at L'Université de Sherbrooke for TGIRT RNA sequencing.

2.3.5 Quality assessment: western blotting of IP samples

Immunoprecipitations were validated via western blotting of inputs, Sla1p IP elutions and rabbit IgG elutions for each stress. Western blotting was conducted as described in section

2.2.3 with the following alterations: electrophoresed samples were transferred to a PVDF membrane instead of nitrocellulose; [1:2000] primary custom antibody, [1:5000] conformation specific mouse α-rabbit secondary antibody, [1:5000] HRP-linked α-mouse IgG tertiary antibody (Cell Signaling Technology cat. #7076S). Blots were stripped and re-probed for β-actin using [1:2500] primary antibody (Abcam cat. #ab8224) and [1:5000] HRP-conjugated α-mouse IgG secondary antibody.

2.3.6 Quality assessment: qRT-PCR of pre-tRNAs

5% of precipitated size-selected RNA for TGIRT RNA sequencing was pelleted, washed, and air-dried as previously described. Air-dried pellets were resuspended in 11 μL of nuclease free H_2O, and concentration was measured using a NanoDrop spectrophotometer (ThermoFisher Scientific). RNA was polyadenylated and converted to cDNA using the qScript microRNA cDNA synthesis kit (Quanta Biosciences) according to the manufacturer's instructions.

5 ng of Sla1p IP and IgG IP cDNA, and 10 ng of input cDNA was used for quantification by qPCR. Forward primers (IDT) and PerfeCta® Universal Reverse PCR primer (Quanta Biosciences) were used at a final concentration of 0.4 μM, and TaqMan™ probes (Integrated DNA Technologies) were used at a final concentration of 0.2 μM. Primer and probe sequences are provided in Appendix A. See Appendix A for a schematic outlining the qRT-PCR design for pre-tRNAs. The reactions were conducted as triplicate technical replicates. Cycling conditions are summarized in **Table 1**. Amplification curves were generated using a Roto-Gene Q machine

(Qiagen). Since amplification curves were sufficient for validating the success of the RNA immunoprecipitations, quantifications and statistical analyses were not performed.

Table 1: qRT-PCR cycle settings for validation of RIP-seq samples.

Cycle Step	Temperature	Duration	Number of Cycles
Initial denaturation	95°C	3 minutes	1
Denaturation	95°C	3 seconds	40
Annealing *and* extension	60°C	20 seconds	
Hold	4°C	∞	n/a

2.4 TGIRT RNA sequencing

2.4.1 Library preparation and sequencing

cDNA libraries for next-generation sequencing were generated using input and Sla1p immunoprecipitated RNA samples at the Université de Sherbrooke RNomics platform using the TGIRT III Sequencing kit/protocol (InGex; https://www.ingex.com/content/Total%20RNA_Enzyme_012317.pdf). Sequencing was performed on an Illumina NextSeq 500 lane for 75 bp paired-end reads.

2.4.2 Analysis pipeline

TGIRT RNA sequencing analysis was conducted by Étienne Fafard-Couture. Details about tools and parameters of bioinformatic analyses are provided in a Snakemake workflow that can be found at https://github.com/etiennefc/S_pombe_RNA_Seq and are also described below. Briefly, paired-end reads were trimmed using Trimmomatic v0.36 (Bolger et al., 2014), and FastQC v0.11.5 was

used to evaluate read quality before and after trimming, as described previously (Fafard-Couture et al., 2021). Resulting trimmed reads were then aligned to the *S. pombe* genome assembly version ASM294v2 using STAR v2.6.1a (Dobin & Gingeras, 2016) (with the parameters described previously (Fafard-Couture et al., 2021)). The index needed to align reads to the genome was produced using STAR v2.6.1a as described previously (Fafard-Couture et al., 2021) using the genome assembly described previously and the genome annotation file (version 56) obtained from PomBase. The annotation file was built by converting the .gff file into a .gtf file using custom bash scripts. This annotation was corrected for embedded genes using CoCo v0.2.5.p1 (Deschamps-Francoeur et al., 2019) with the correct_annotation mode and default parameters. Counts were attributed to genes and normalized as transcripts per million (TPM) as previously described (Fafard-Couture et al., 2021) using CoCo v0.2.5.p1 with the correct_count mode.

Bedgraph files were generated using CoCo v0.2.5.p1 (with the correct_bedgraph mode with default parameters). Differential expression analysis was performed using DESeq2 (Love et al., 2014) with default parameters and the count output of CoCo correct_count to compare the wild type versus the *sla1* knockout samples, the different stress input samples against each other and the different IP samples against each other. Ratios of ratios (RoR) (i.e., (IP stress / input stress) / (IP normal / Input normal)) were also computed for each gene and a likelihood ratio test was applied to verify the statistical significance in differences of RoR between stress and wild type conditions.

tRNA read fishing and binning was conducted by Étienne Fafard-Couture with assistance from Kyra Kerkhofs. Raw counts for pre-tRNA (3'-UUU) and mature tRNAs (3'-CCA) were

generated using custom python scripts. A list of unique sequences was generated for each tRNA isoacceptor and used to obtain ("fish") all reads from the unmapped raw sequence files (.fastq file format). Each sequence was grouped in corresponding bins based on the 3'-end of the reads: -CCA (mature tRNA), 1U, 2U, 3U, 4U, 5U, 6U, 7U, 8U, 9U or 10U (premature tRNA). Raw counts for each tRNA isotype were normalized as counts per million (CPM) by dividing raw counts by the total number of fished read per bin for each replicate divided by 10^6.

2.5 RIP-seq validations

2.5.1 Northern analyses

DNA oligonucleotide probes (see Appendix A) were radioactively labelled on the 5'-end using γ-^{32}P-ATP. The 10 μL labelling reaction consisted of: 0.5 μL of T4 polynucleotide kinase (PNK) (New England Biolabs cat. #M0201S), 1 μL of 10X PNK buffer (New England Biolabs cat. #B0201S), 2.5 μM probe oligonucleotide (Integrated DNA Technologies), 1 μL γ-^{32}P-ATP (Perkin Elmer, 10 mCi/mmol), and 7 μL nuclease-free H_2O. The reaction was incubated at 37°C for 2 hours, followed by 5 minutes at 95°C for PNK inactivation.

Precipitated RNAs from repeated immunoprecipitations were prepared as described in section 2.3.4. 15 μg of input RNA and 100% of Sla1p IP and IgG IP RNA were resolved on a 12% denaturing urea gel (8 M urea, 12% acrylamide, 1X TBE) at 100 V until the bromophenol blue dye front migrated off the gel. Following electrophoresis, the samples were transferred to a nylon membrane using the iBlot 2 Dry Blotting System (Invitrogen) according to the manufacturer's instructions and cross-linked to the membrane using the Fotodyne DNA Transfer Lamp for 90 seconds. Following UV cross-linking, the membrane was dried at 80°C for

15 minutes using a gel dryer (BioRad). The membrane was then incubated in 20 mL of pre-hybridization buffer (6X SSC, 2X Denhardt's solution, 1% SDS, 2 mg yeast RNA) at 10°C below the melting temperature (T_m) of the probe for 2.5 hours. Following pre-hybridization, 10 μL of radioactively labelled probe was added to the pre-hybridization buffer, and the membrane was probed overnight in a rotating hybridization oven at 10°C below T_m. The membrane was subsequently washed three times for 20 minutes with Wash Buffer (2X SSC, 0.1% SDS), with the first wash occurring at probing temperature, and the second and third at room temperature. Signal was detected by exposing the membrane to a storage phosphor screen overnight and imaged using a Typhoon scanner (General Electric).

For re-probing, the membrane was stripped by washing three times for 20 minutes in Stripping Buffer (0.1X SSC, 0.1% SDS) at 70°C.

2.5.2 H_2O_2 time course

Wild-type and Δ*sla1 S. pombe* cells were grown in 250 mL of YES media at 32°C until mid-log phase. 50 mL of each culture was decanted prior to applying oxidative stress to serve as timepoint 0 minutes. Oxidative stress was applied to the remaining 200 mL of each culture as described in section 2.3.1. After 30, 60, and 180 minutes post-stress induction, 50 mL of each culture was harvested and subjected to hot phenol RNA extraction as described in section 2.3.3. Precipitated RNA was prepared as described in section 2.3.4, and 15 μg of each sample was resolved on a 12% denaturing urea gel at 100 V until the bromophenol blue dye front migrated off the gel. Northern blotting was performed as described in section 2.5.1.

2.6 Oxidative stress survival and growth assays

2.6.1 Spot assay

Biological triplicates of wild-type and Δ*sla1 S. pombe* cells were grown in 10 mL of YES media at 32°C until mid-log phase. All cultures were seeded to OD_{600nm} = 0.6 in 250 μL of YES media in order to equalize the number of cells in stock cultures. 10-fold serial dilutions were prepared in a sterile 96-well plate and a pronged replica plater (Sigma-Aldrich) was used to spot the dilutions on YES agar plates containing either 0, 1, or 2 mM H_2O_2. Spots were air-dried beside a flame and were grown at 32°C for two days.

2.6.2 Streaking assay

Wild-type and Δ*sla1 S. pombe* strains were streaked on YES agar plates and grown at 32°C until visible colonies formed (about three days). Two comparable colonies of each strain were picked with sterile pipette tips and streaked on YES agar plates containing either 0, 1, or 2 mM H_2O_2. Plates were grown at 32°C for two days.

CHAPTER 3: RESULTS

3.1 Successful generation of α-Sla1p antibody

In order to raise a custom polyclonal antibody against Sla1p, the protein was recombinantly expressed, purified, and injected into rabbit models as a target antigen. The *sla1* gene with a C-terminal 6x-His tag was previously cloned into the pET23a vector and expressed in *E. coli* using standard methods. Taking advantage of the 6x-His tag, Sla1p was purified from the bacterial cell lysate using Ni^{2+} affinity chromatography. Aliquots from each step of the purification were collected and resolved on an SDS-PAGE gel for visualization and concentration estimation (**Figure 3.1**).

Most non-specific proteins passed through the column and were collected in the flow-through, while any that were retained in the column were eluted during the first wash. The loss of some Sla1p (approximately 40 kDa) in each of the five washes as well as intense signal in each of the two elution lanes suggest robust Sla1p expression and saturation of the column (**Figure 3.1A**).

According to their '2 rabbit, 90 day' protocol, Pierce Proteomics required a total of 1.7 mg of affinity-purified antigen for the primary and boost immunizations. As such, the concentration of purified Sla1p was estimated using densitometry analysis against BSA standards. To conduct this analysis, 0.05, 0.1, 0.25, and 0.5 μL of concentrated Sla1p was resolved on an SDS-PAGE gel alongside 1, 2, 4, and 8 μg of BSA standard (**Figure 3.1B**). Following Coomassie staining, it was found that the intensity of the 0.25 μL Sla1p signal was

comparable to that of 2 μg BSA, indicating a final concentration of approximately 2 μg/0.25 μL, or 8 μg/μL. Therefore, the 500 μL sample of concentrated protein sent to Pierce Proteomics for antigen immunization contained approximately 4 mg of purified Sla1p. Rabbits were bled on the 72nd day of the protocol, and the α-Sla1p antibody was purified from obtained sera via affinity chromatography using purified Sla1p as an immobilized ligand. Since an additional 5 mg of antigen was required for affinity purification of the antibody, an identical Sla1p purification was conducted (data not shown) to obtain the additional Sla1p.

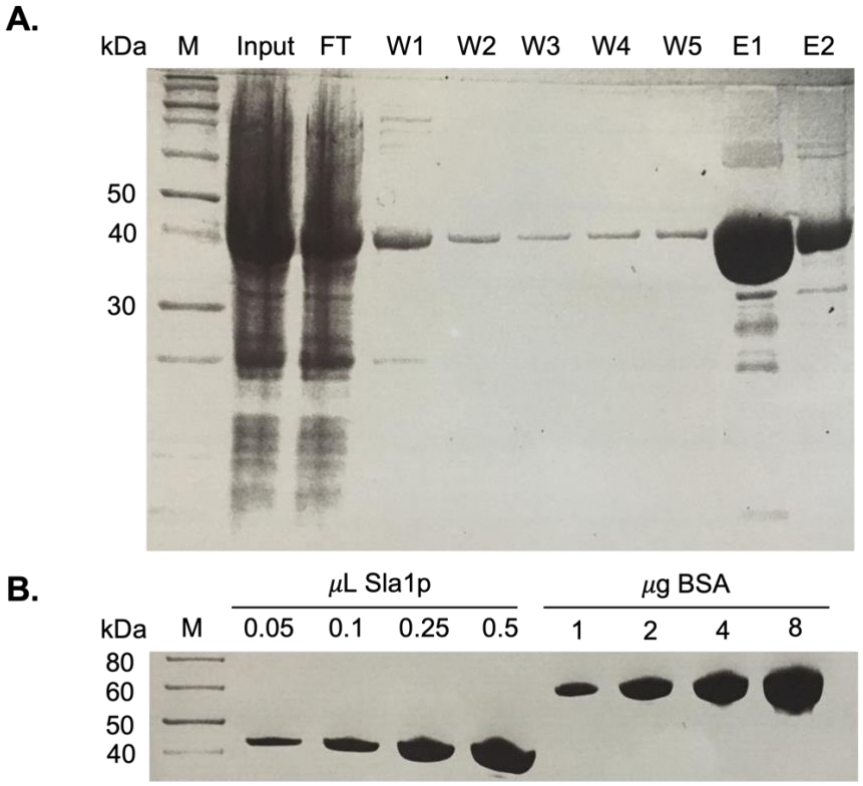

Figure 3.1: Affinity purification and concentration estimation of Sla1p. (A): Recombinant 6x-His tagged Sla1p was expressed and purified from BL21 *E. coli* cells using Ni^{2+} affinity chromatography. The column was washed (W1-5) using a buffer with low imidazole concentration (20 mM) and the retained Sla1p was eluted (E1, E2) from the column using a competing concentration of imidazole (300 mM). FT = flow-through (B): The concentration of purified Sla1p was estimated visually using densitometry analysis against known BSA standards. Sla1p concentration was estimated to be about 8 μg/μL.

Two bottles containing 11 mL of affinity-purified custom α-Sla1p antibody were received from Pierce Proteomics, each corresponding to polyclonal antibody produced by one of the two rabbit models (**Figure 3.2**). The first antibody (AB2596) was purified to a final concentration of 1.58 mg/mL, while the second antibody (AB2597) was purified to 1.68 mg/mL. Since two unique polyclonal antibodies were obtained, all downstream validations and optimizations were performed in duplicate; one replicate per antibody.

Figure 3.2: Affinity-purified custom α-Sla1p polyclonal antibody. Custom α-Sla1p polyclonal antibody was raised by Pierce Proteomics (ThermoFisher Scientific). Affinity-purified Sla1p antigen was injected into two rabbit models who produced polyclonal antibodies against Sla1p over 72 days. The custom antibody was purified from rabbit blood sera via affinity purification using Sla1p as an immobilized ligand on a column.

3.2 α-Sla1p is functional in immunodetection assays

The custom antibodies were validated via western blotting targeting either endogenous or exogenous Sla1p in various *S. pombe* strains (**Figure 3.3**). Total cell lysates were prepared for each strain and transformant, and western blots were conducted to assess the antibodies' specificity by using custom α-Sla1p as primary antibody. Purified Sla1p was included as a positive control.

In the initial validation, primary antibody was used at a 1:1000 dilution, as per the recommendation of Pierce Proteomics. Using this dilution, AB2596 appropriately detected purified Sla1p at about 40 kDa (**Figure 3.3A**, lane 9). Additionally, endogenous Sla1p was detected as expected in both the WT and WT* strains (lanes 1 and 3). The WT strain is an unmodified wild-type strain, while WT* contains Protein A-tagged Slr1 (*S. pombe* La-related protein 1) but is wild-type with respect to *sla1*. Further validating the specificity of the antibody, Sla1p was not detected in the Δ*sla1* strain (lane 2). A Protein A-tagged Sla1p yeast strain was previously generated by integrating an in-frame Protein A tag to the C-terminus of Sla1p via homologous recombination as previously described (Wang et al., 2017). As a result, endogenous transcription from the Sla1p genomic locus would result in a Sla1p-Protein A fusion protein approximately 20 kDa greater in molecular weight than Sla1p. Accordingly, Sla1p was detected at an increased molecular weight (approximately 60 kDa) in the Protein A-tagged Sla1p strain (lane 4).

The *S. pombe* transformants also provided information regarding the efficacy of the antibody in immunodetection. Sla1p was detected in WT cells transformed with the empty pRep4 vector comparable to untransformed WT cells (compare lanes 1 and 5), as well as in overexpressed amounts in the WT strain transformed with pRep4-*sla1* (compare lanes 1, 5, and 6). In contrast, Sla1p was not detected in the Δ*sla1* strain transformed with the empty vector (lane 7), yet expression was rescued when transformed with pRep4-*sla1* (lane 8). Blotting with AB2597 yielded similar results, however, in all lysate-containing lanes a non-specific protein of approximately 50 kDa was detected that was not detected using AB2596 (**Figure 3.3B**), suggesting lower specificity compared to AB2596. Interestingly, this non-specific protein was not detected in the lane containing purified Sla1p, suggesting it is recognizing an endogenously expressed *S. pombe* protein. It was also still present in Δ*sla1* strains (lanes 2 and 7), suggesting its detection is independent of Sla1p.

Following this validation, primary antibody dilution for western blots was optimized. Subsequent attempts of the same western analysis were performed using 1:2000 and 1:10,000 dilutions for each primary antibody. Secondary antibody dilution was maintained at 1:5000 to provide confidence that the primary antibody dilution influenced any variable signal. Adequate detection of Sla1p was obtained using both dilutions, although diminished detection of Sla1p degradation products using the 1:10,000 dilution decided that all downstream western analyses would be conducted using a 1:2000 dilution of primary antibody. Subsequent unrelated western blots (not shown) indicated that 1:5000 is also an acceptable primary antibody dilution.

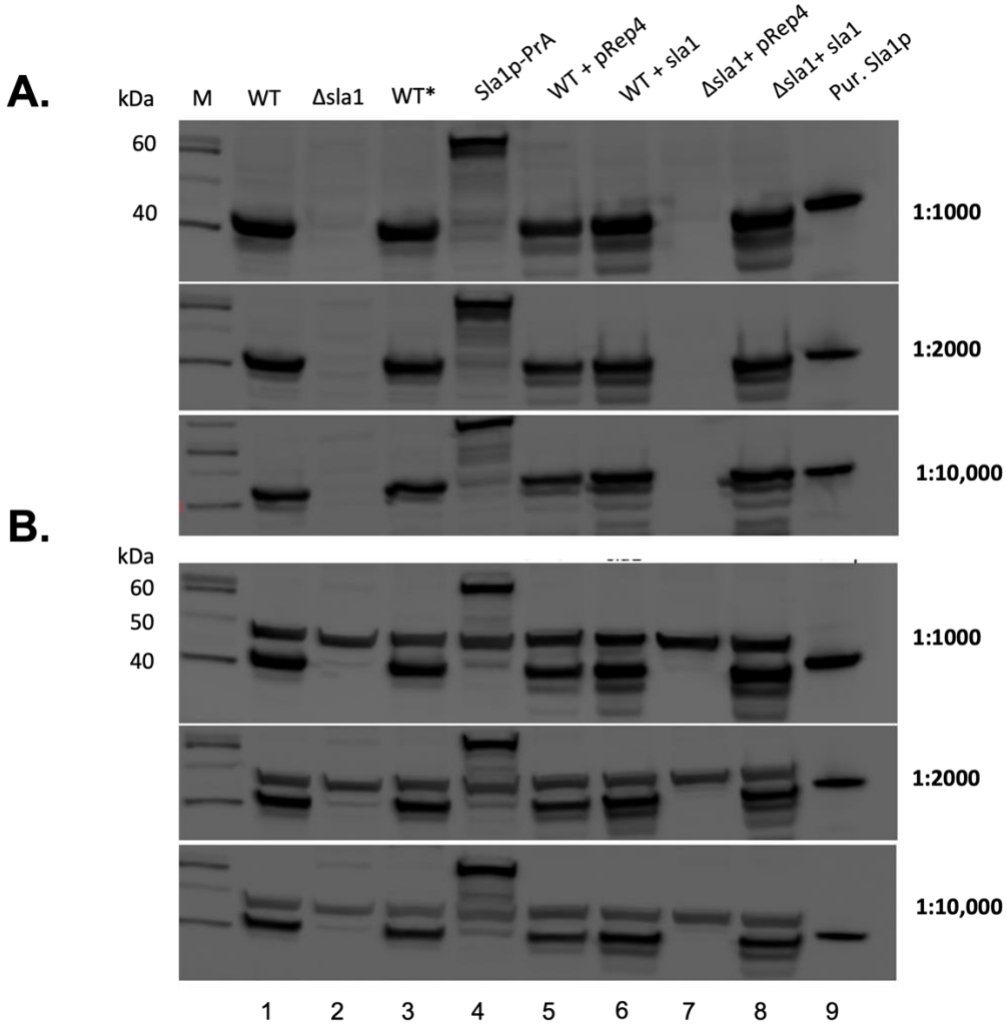

Figure 3.3: Western blots validating custom α-Sla1p antibody and optimizing primary antibody dilution. Endogenous and/or recombinantly introduced Sla1p was detected from yeast whole cell lysates using either AB2596 (A) or AB2597 (B). Initial validation was conducted using a primary antibody dilution of 1:1000. Subsequent attempts for primary antibody dilution optimization were conducted at 1:2000 and 1:10,000. WT = wild-type, WT* = yeast strain containing Protein A-tagged *S. pombe* La related protein 1, but wild-type with respect to *sla1*. Pur. Sla1p = purified Sla1p protein. Marker indications for each blot are identical.

The performance of the custom α-Sla1p antibodies was further assessed and optimized for immunoprecipitations. Endogenous Sla1p was immunoprecipitated from either wild-type or

Δ*sla1 S. pombe* cells using AB2596 and AB2597. Each IP was conducted with 0.2 g of yeast cell grindate, and two Protein-A-Dynabead volumes were assessed: 25 μL and 50 μL. Since Protein-A-Dynabeads have a binding capacity of approximately 100 μL beads:30 μg antibody (per the manufacturer), these ratios were kept constant and therefore approximately 8 μg and 16 μg of α-Sla1p were used respectively. Samples from each input, flow-through, and immunoprecipitate were assessed by western blot (**Figure 3.4**). The primary antibody used for western analysis was the same as that used for the IP.

Sla1p was successfully immunoprecipitated in IPs conducted in wild-type cells, and not immunoprecipitated in the Δ*sla1* strain, suggesting that our custom antibodies function specifically in IP assays. The use of greater bead and antibody volumes allowed for in increased immunoprecipitated Sla1p. Downstream IPs were therefore maintained at 50 μL beads and 16 μg α-Sla1p in order to maximize RNP pulldown. Sla1p detected in the flow-through (FT) lanes of the wild-type IPs suggested an excess of unbound Sla1p, and thus was of primary interest during downstream optimization. The band in each IP lane greater in molecular weight than Sla1p corresponds to detected heavy chain of the α-Sla1p antibody. This was resolved in future western blots by using a conformation-specific secondary antibody that only detects intact IgG. Similar results were obtained with AB2597. Finally, the 50 kDa non-specific protein previously found to interact with AB2597 was detected in the input and FT lanes of both wild-type and Δ*sla1* cells, along with a second non-specific protein slightly greater in molecular weight than Sla1p. However, these non-specific proteins are not detectable in each IP lane. This is consistent with the denatured (by SDS-PAGE) non-specific endogenous proteins being recognized by

AB2597 by western, but the native versions of these proteins not being immunoprecipitated. This observed difference in affinity for the non-specific proteins by AB2597 in western blots versus IPs is addressed further in Chapter 4. Ultimately, these data suggest excellent antigen affinity for α-Sla1p during immunoprecipitation.

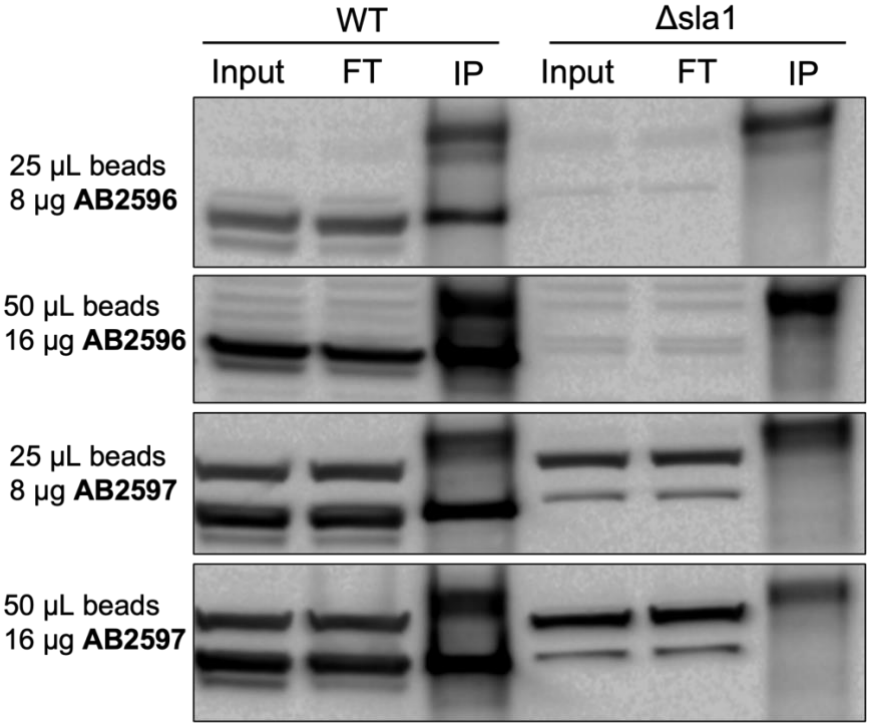

Figure 3.4: Western blot of Sla1p immunoprecipitation using the custom α-Sla1p antibodies. Endogenous Sla1p was immunoprecipitated from wild-type (WT) and Δsla1 *S. pombe* cells using either AB2596 or AB2597. Lysate for each immunoprecipitation was prepared using 0.2 g of yeast cell grindate. Protocol optimization was attempted by conducting each immunoprecipitation using either 25 µL or 50 µL of Protein A-Dynabeads. Quantity of conjugated antibody was determined according to the binding capacity of the Dynabeads stated by the manufacturer. Samples from each input, flow-through (FT) and immunoprecipitate (IP) were analyzed via western blot using the IP antibody as primary.

As optimal amounts of beads and α-Sla1p were previously established, further IP optimization focussed on decreasing unbound Sla1p in the flow-through while enriching Sla1p

in the IP (**Figure 3.5**). To do this, the amount of yeast grindate used per immunoprecipitation was reduced to 0.1 g and 0.02 g – 50% and 10% of the previous amount used, respectively. Although Sla1p accumulation in the FT was reduced using 0.1 g of grindate compared to the initial 0.2 g, this effect was greater using 0.02 g of grindate, where no Sla1p was present in the FT (**Figure 3.5A**). Although 0.02 g of grindate seemed to provide optimal IP results through western blot, it was essential to also be able to detect co-immunoprecipitated RNAs in parallel, namely, pre-tRNAs. Therefore, levels of co-immunoprecipitated RNAs from each amount of grindate were assessed by northern blot (**Figure 3.5B**). Precursor and mature isoforms of tRNA Lys^{CUU} were targeted using probes specific to the intron and processed 3' end, respectively. In IPs conducted with 0.1 g of grindate, pre-tRNA Lys^{CUU} was detected in the immunoprecipitates. In contrast, pre-tRNA Lys^{CUU} was not detected in IPs using 0.02 g of grindate, due to already low abundance in cells and small lysate volume. From both grindate amounts, the mature isoform was less efficiently immunoprecipitated than the precursor as demonstrated by lack of enrichment of mature tRNA Lys^{CUU} in the IP versus the input. There did not seem to be a noticeable difference in co-immunoprecipitated RNAs between AB2596 and AB2597. Finally, the La-non-target U5 snRNA was blotted as a negative control. Lack of enrichment of U5 snRNA in the IP versus the input indicated minimal interaction with Sla1p *in vivo* and justified its use as a negative control. Altogether, these data prompted downstream IPs to be conducted with 0.1 g of grindate, 50 μL of beads, and 16 μg of antibody. For IPs conducted to prepare samples for sequencing, twice the amount of grindate, beads, and antibody were used in order to maximize RNA available for sequencing.

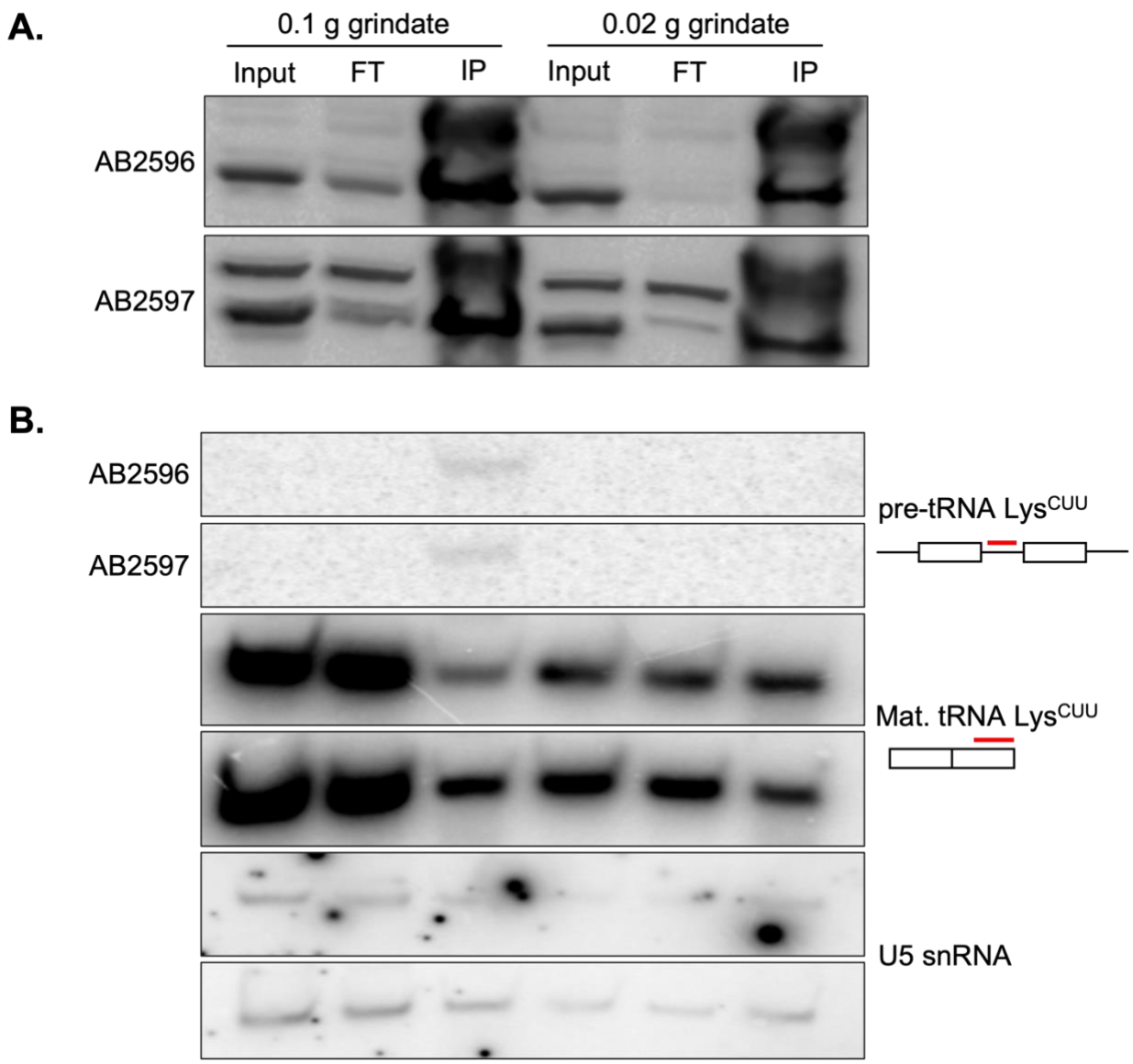

Figure 3.5: Optimization of Sla1p immunoprecipitation. Endogenous Sla1p was immunoprecipitated from the WT* strain using either AB2596 or AB2597. 50 μL of Protein A-Dynabeads and 16 μg of each antibody was used for each IP with either 0.1 g or 0.02 g of grindate. Western blots depicted in (A) using IP antibody as primary. Co-immunoprecipitated RNAs were analyzed by northern blot (B). tRNA isoforms were detected with radiolabelled probes according to the legend. The La-non target U5 snRNA was probed as a negative control. Pre-tRNA Lys^{CUU} was only noticeably enriched in each IP from 0.1 g of grindate.

3.3 Optimization of RNA size selection prior to sequencing

Prior to TGIRT RNA sequencing, co-immunoprecipitated RNAs needed to be depleted of overly abundant RNAs that would take up most of the reads, namely rRNAs. This proved to be challenging for our specific application since rRNA depletion is commonly performed by enrichment of poly(A)-containing transcripts, as most RNA-seq work focuses on mRNAs. Since our interest was within the cohort of RNAs transcribed by RNAP III, poly(A) enrichment was not a viable option for transcript selection. Additionally, rRNA depletion kits are not commercially available for *S. pombe*. Therefore, RNAs of interest were size selected, and rRNAs were depleted by gel extraction.

In order to optimize this method, input, Sla1p-associated, and IgG-associated RNAs were resolved on a denaturing urea gel. Following staining with ethidium bromide, the gel was viewed under UV light to guide cutting (**Figure 3.6A**). In each lane, two distinct bands were observed, the larger corresponding to 5.8S rRNA and the smaller to 5S rRNA. The optimization aimed to retain RNAs that would be of interest during sequencing (ie. tRNAs), while minimizing overly abundant RNAs that were not of particular interest (ie. rRNAs). Since 5S rRNA is the only rRNA transcribed by RNAP III, we suspected it may interact with Sla1p. Therefore, we attempted two distinct gel cutting patterns, indicated in **Figure 3.6** as either “1” or “2”. With pattern 1, the gel was cut above the 5.8S rRNA band such that both types of rRNA were retained for the RNA extraction, and with pattern 2, the gel was cut below the 5S rRNA band such that both types of rRNA were not included for RNA extraction. Although not shown in **Figure 3.6A**, the same cutting patterns were used for both Sla1p IP RNA and IgG RNA. RNAs

within the gel were extracted overnight with phenol:chloroform:isoamyl alcohol and precipitated with ethanol. The newly precipitated RNA was then subjected to northern analysis to assess the value of each cutting pattern (**Figure 3.6B**). The known Sla1p target, pre-tRNA Lys^{CUU} was only detected in Sla1p IP cut with pattern 1, suggesting that cutting pattern 2 was inadequate, as we wanted to retain pre-tRNAs for sequencing. Similarly, U5 snRNA, which may interact with Sla1p, was only detectable in the Sla1p IP with pattern 1. 5S rRNA was blotted for as a control and was appropriately only detected in lanes cut with pattern 1. These results prompted us to cut between the two rRNA bands for the final RIP-seq such that pre-tRNAs, U5 snRNA, and 5S rRNA were retained, but other unnecessary larger RNAs were not.

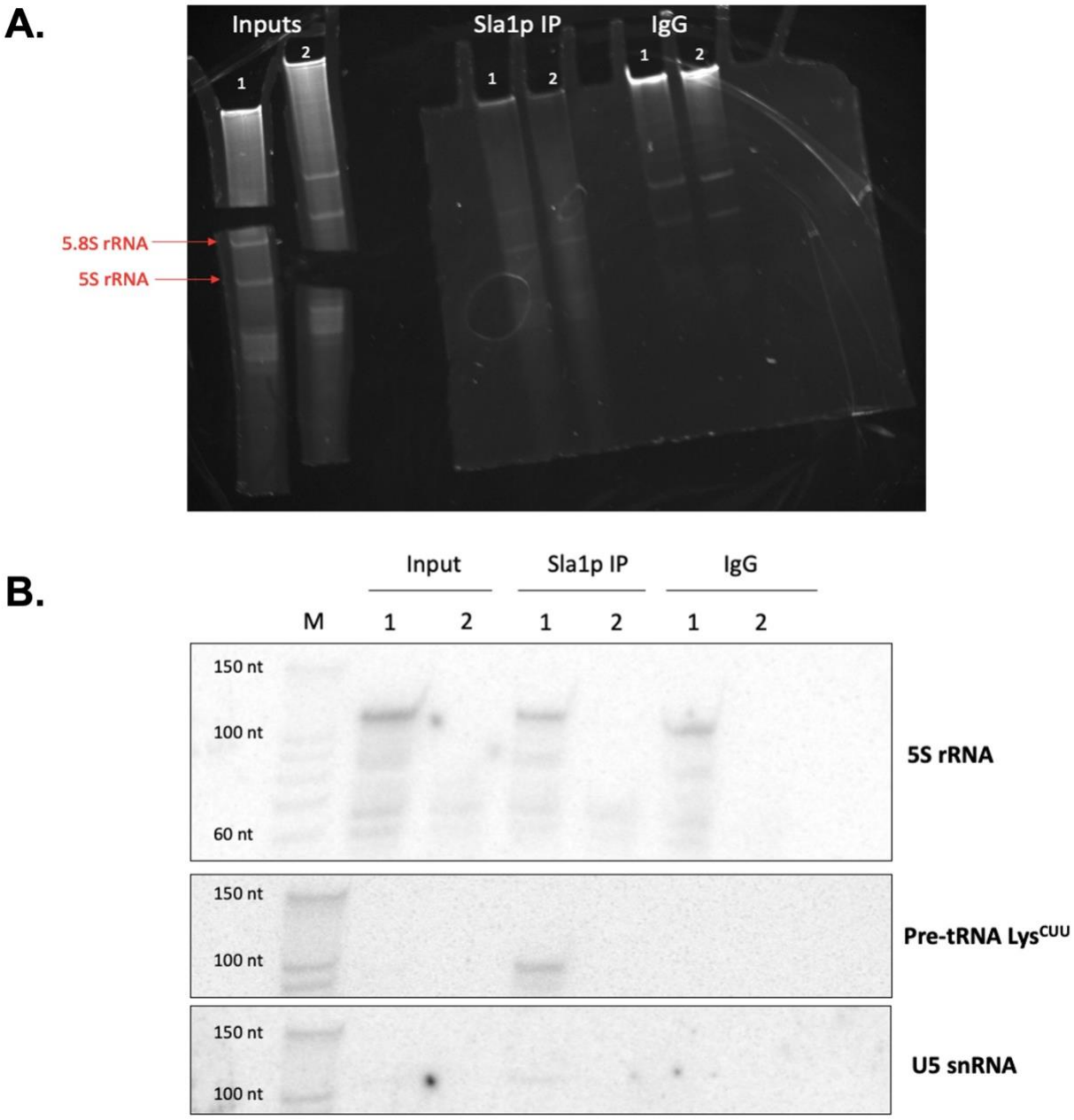

Figure 3.6: Optimization of rRNA depletion gel extraction. Following Sla1p immunoprecipitation from normally grown cells, RNA from the input, Sla1p IP, and IgG control were resolved on a denaturing urea gel for size exclusion (A). Each RNA sample was split equally into two lanes to assess the efficacy of two distinct gel cutting patterns (1 and 2). Each cutting pattern was used consistently across RNA samples, and the bottom half of the cut gel was retained for RNA extraction from the gel. Following gel extraction, precipitated RNA was subjected to northern analysis with probes targeting 5S rRNA, pre-tRNA Lys^{CUU} and U5 snRNA (B).

3.4 Quality assessment of TGIRT RNA sequencing samples

Prior to sending the size-selected RIP samples for sequencing, their quality was validated by assessing pre-tRNA levels using TaqMan qRT-PCR. (**Figure 3.7**) For all stresses, Sla1p IP samples displayed satisfactory amplification of the pre-tRNA, while inputs and IgG negative controls did not. Minimal amplification of pre-tRNA in the inputs was hypothesized to be a consequence of relatively low abundance due to rapid processing in the cell. Minimal signal in the IgGs once again confirmed that α-Sla1p has specific and high affinity for Sla1p. Fold enrichment quantitation was therefore made difficult by the minimal amplification in inputs and IgGs. As such, the amplification curves were used as a visual tool to validate the samples and revealed expected enrichment of pre-tRNAs in the Sla1p IPs relative to both the inputs and IgGs. These results indicated that the RIP was successful and justified sending the samples to our collaborators at L'Université de Sherbrooke, who later confirmed that the cDNA libraries (prepared by them) were suitable for sequencing. It is necessary to note that RNAs associated with IgG IPs were not sent to our collaborators as it was suspected that they were too lowly abundant for cDNA library preparation.

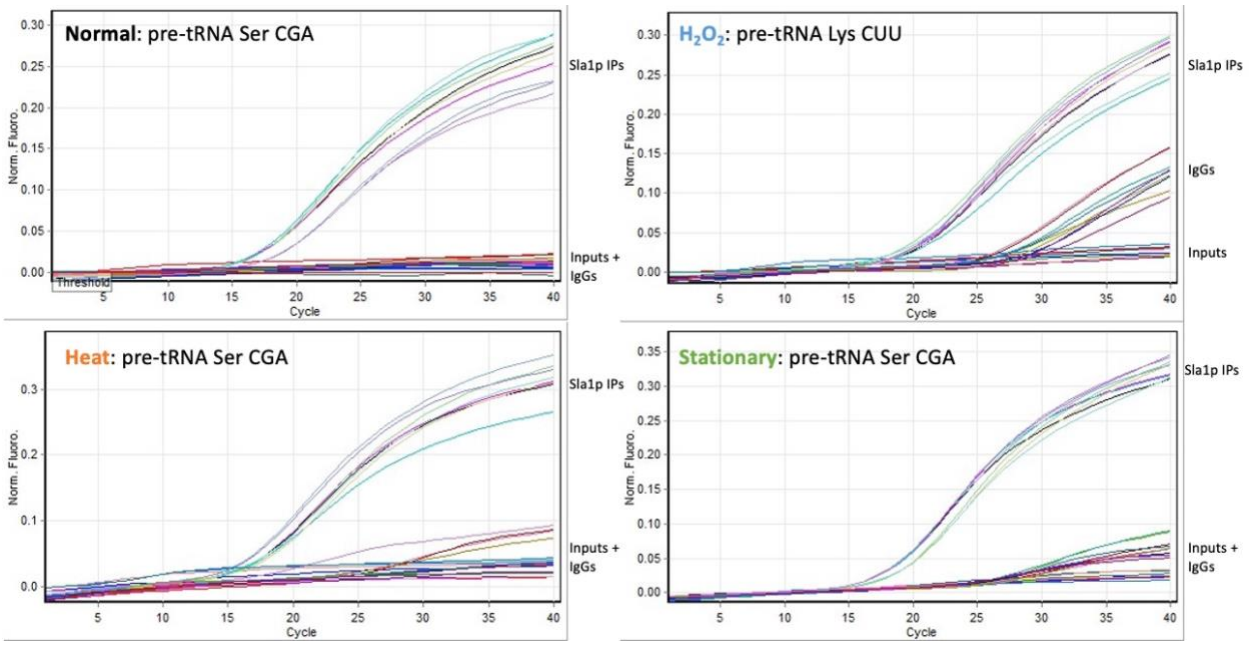

Figure 3.7: qRT-PCR validation of co-immunoprecipitated RNAs for sequencing. Input, Sla1p IP, and IgG IP RNAs from all stresses were size selected and validated by qRT-PCR prior to sending to collaborators for sequencing. The pre-tRNA targeted for each qRT-PCR run is specified for each stress on the respective graph. For all stresses, Sla1p IP samples displayed satisfactory enrichment of pre-tRNA relative to inputs and IgG controls. The results justified sending the RNA samples to our collaborators for sequencing.

3.5 Sla1p does not differentially engage pre-tRNAs during stress

For all cellular conditions, input and Sla1p IP-associated RNAs were prepared by our collaborators for 75 nucleotide paired-end RNA sequencing using the thermostable group II intron reverse transcriptase (TGIRT). Prior to analysis, targets were filtered to remove genes with less than 1 transcript per million in any of the input samples. DESeq2 was then used to filter out genes with highly variable expression across replicates. Differential expression/enrichment analysis was conducted by our collaborators in order to identify RNAs whose interaction with Sla1p is altered during cellular stress. That is, a ratio of ratios (RoR) was

calculated as below, with interesting targets having a fold enrichment value *not* equal to 1 after normalizing for potential differences in expression.

$$Fold\ enrichment = \frac{\frac{Stress\ Sla1p\ IP}{Stress\ input}}{\frac{Normal\ Sla1p\ IP}{Normal\ input}}$$

The volcano plots below highlight the RoRs for each target versus the negative log of the false discovery rate-adjusted p-value during each stress (**Figure 3.8**). For each plot, targets at the extremes of the x-axis are differentially associated with Sla1p during stress, and hits above the line y = 1.3 represent statistical significance ($p_{adj.} \leq 0.05$). Therefore, points residing in the upper right quadrant represent targets that would engage Sla1p more during stress – aligning with our hypothesis, while points in the upper left would represent targets that engage Sla1p less during stress. Interestingly, there were no tRNAs that displayed significantly increased interaction with Sla1p during cellular stress – excluding the one tRNA hit in stationary phase stress corresponding to tRNA Ile that had highly variable reads, and for unclear reasons was not successfully filtered by DESeq2 (**Figure 3.8C**). Additionally, both heat and stationary phase stress did not yield increased interaction with Sla1p for any RNA subtype (**Figure 3.8B & C**) Therefore, the results obtained from the RIP-seq experiment did not align with our hypothesis that La might preferentially bind certain targets during stress but were consistent with our previous work indicating that La does not preferentially engage misfolded RNA substrates (Vakiloroayaei et al., 2017).

Expanding the analysis to all targets, few transcripts reached a statistically significantly different Sla1p enrichment upon stress treatment. H_2O_2 stress resulted in the most statistically significant hits, the majority of which were mRNAs (**Figure 3.8A**). The RNAs that significantly increased their interaction with Sla1p under H_2O_2 stress were primarily ribosomal protein mRNAs (RoR > 1 and $p_{adj.} \leq 0.05$), while those that significantly decreased their interaction with Sla1p were primarily mitochondrially encoded mRNAs (RoR < 1 and $p_{adj.} \leq 0.05$) (Appendix B, **Supplementary Table 1**). From the raw sequencing data, it was clear that reads for the ribosomal protein mRNAs generally were not changed by H_2O_2 stress in the inputs but did increase in the Sla1p IP. In contrast, the mitochondrially encoded mRNAs were also not changed by H_2O_2 stress in the inputs but decreased in the Sla1p IP. Validation of these unexpected results by qRT-PCR was explored on a preliminary basis (data not shown) and therefore remains an interesting prospect for future work.

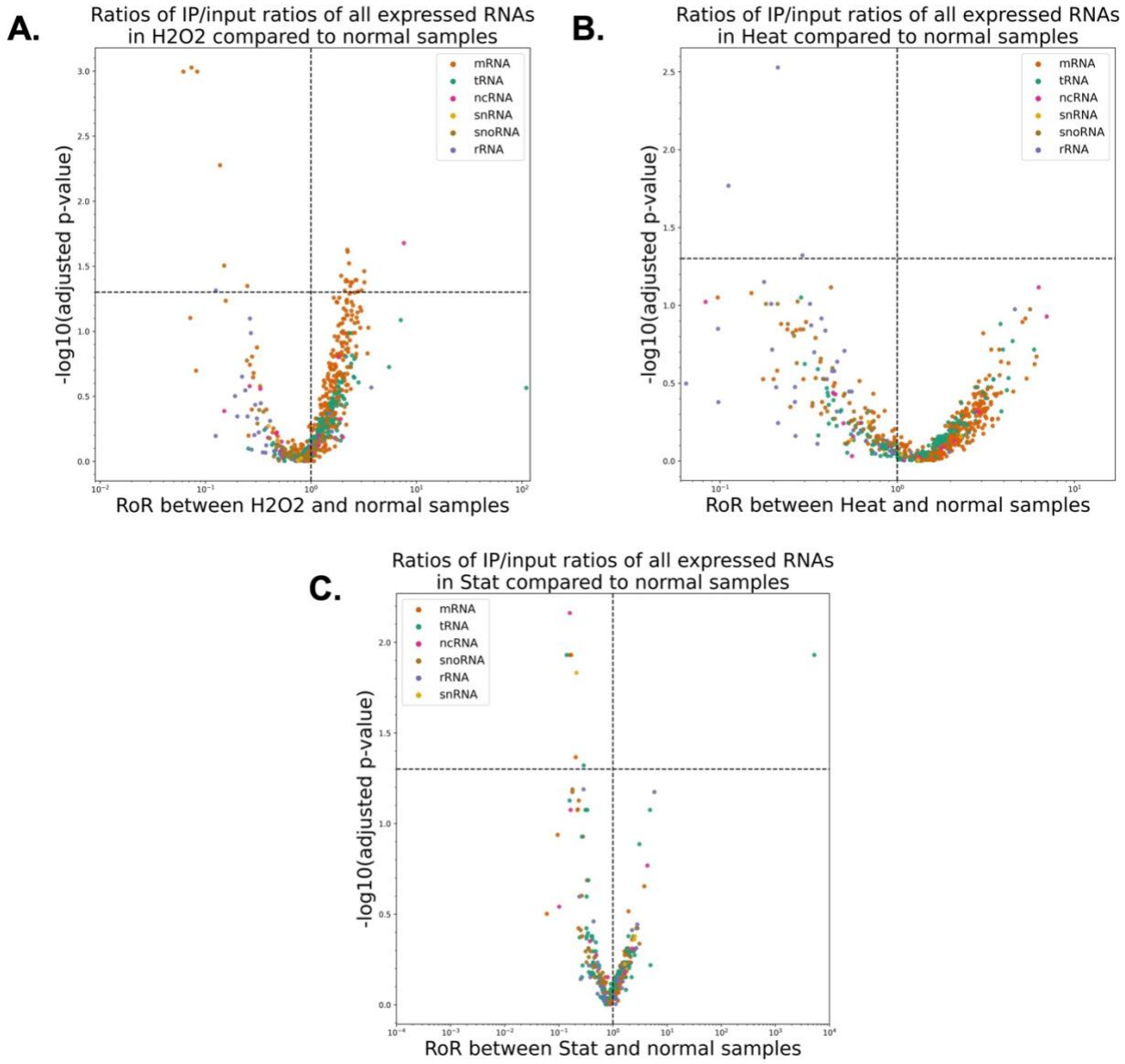

Figure 3.8: Volcano plots depicting altered interaction between Sla1p and RNAs under cellular stress. TGIRT-RNA sequencing was performed on input and Sla1p IP samples from normal and stressed *S. pombe* cells. Differential expression analysis for each gene was conducted by calculating a ratio of ratios (RoR) between the Sla1p IP / input of each stress relative to the Sla1p IP / input ratio for the normal samples. The RoRs for each gene were plotted against the negative log of the adjusted p-value for each stress (A: H_2O_2, B: Heat, C: Stationary phase). Sla1p's association with tRNAs was not altered by cellular stress. H_2O_2 stress resulted in increased association between Sla1p and select ribosomal protein mRNAs, and decreased association with select mitochondrially encoded mRNAs. Plots generated by Étienne Fafard-Couture.

3.6 Various pre-tRNAs undergo altered processing during H_2O_2 and stationary phase stress

In order to validate the null result obtained for tRNAs in the RIP-seq, additional RIPs were conducted in three independent biological replicates for each cellular condition and followed up with northern blots (**Figure 3.9**). Interestingly, when using a probe specific to the intron of pre-tRNA Lys^{CUU}, we observed enrichment for the leader-processed intermediate in the H_2O_2 Sla1p IP that was not evident for the other stresses. Under normal conditions, Sla1p associated more with the nascent, end-unprocessed transcript, consistent with its established role in 3' end protection of pre-tRNAs during maturation. The leader-processed intermediate was similarly enriched in the H_2O_2 input compared to the non-stressed condition. Additionally, stationary phase stress resulted in enriched interaction between Sla1p and the nascent transcript compared to normal conditions. While the nascent transcript was also the most associated with Sla1p under normal conditions, its abundance relative to other intermediates was noticeably enhanced during stationary phase stress. The pre-tRNA Lys^{CUU} nascent transcript was not visible in the input lanes, so conclusions about the global effect of stress on expression and processing cannot be made from the northern blot. Under all cellular conditions, Sla1p associated least with the fully processed, intron-containing transcript, once again consistent with La-dependent tRNA processing. Finally, the percent abundance of each pre-tRNA Lys^{CUU} intermediate associated with Sla1p was quantified for each stress and compared to normal conditions for statistical validation (**Figure 3.10**). Overall, this quantification confirmed the significance of observed differences in pre-tRNA Lys^{CUU} intermediates associated with Sla1p under H_2O_2 and stationary phase stress.

In order to address whether the altered interaction between Sla1p and pre-tRNA processing intermediates during stress was a phenomenon unique to Lys^{CUU}, we also probed for pre-tRNA Ser^{UGA} and pre-tRNA Val^{AAC}. Interestingly, their processing intermediates were found to interact with Sla1p in a similar distribution as pre-tRNA Lys^{CUU} during H_2O_2 and stationary phase stress. It is necessary to note that sufficient separation of the pre-tRNA Val^{AAC} intermediates was not observed in two of the three replicates despite the same or higher acrylamide concentration in the gel, and pre-tRNA Ser^{UGA} was only probed from one biological replicate.

Finally, an intron-less pre-tRNA species, Asn^{GUU} was also targeted in order to address whether the observed stress-related changes to pre-tRNA processing is specific to intron-containing species. H_2O_2 stress similarly resulted in increased Sla1p association with leader-processed transcript compared to normal conditions. Interestingly, stationary phase stress also resulted in increased Sla1p association with leader-processed transcript, rather than primary transcript as was the case for the intron-containing pre-tRNAs tested. Overall, these data suggest that H_2O_2 and stationary phase stress result in altered pre-tRNA processing and association of processing intermediates with Sla1p.

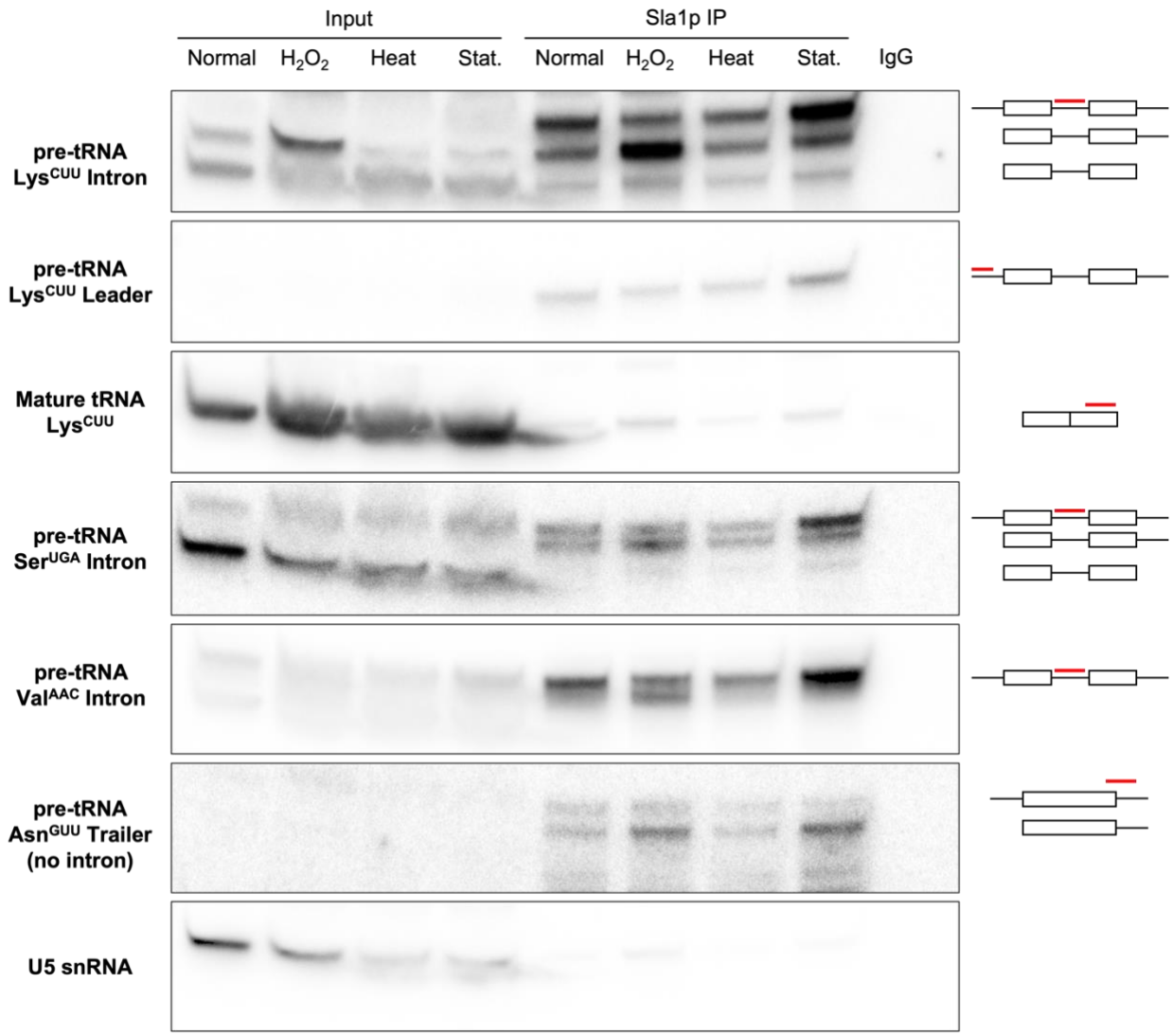

Figure 3.9: Northern blot of RNA in input and co-immunoprecipitated by Sla1p during stress. Endogenous Sla1p was immunoprecipitated from wild-type *S. pombe* cells under normal, and stress conditions using AB2597. Input and co-immunoprecipitated RNA were resolved on a denaturing urea gel and subjected to northern analysis. Various RNA species were probed for using radiolabelled oligonucleotides that anneal to the targets according to the legend. An IP conducted with non-immune rabbit IgG from normally grown cells was included as a negative control. H_2O_2 and stationary phase stress result in altered processing and association of pre-tRNA intermediates with Sla1p compared to normal conditions. The most representative figure was chosen from three biological replicates.

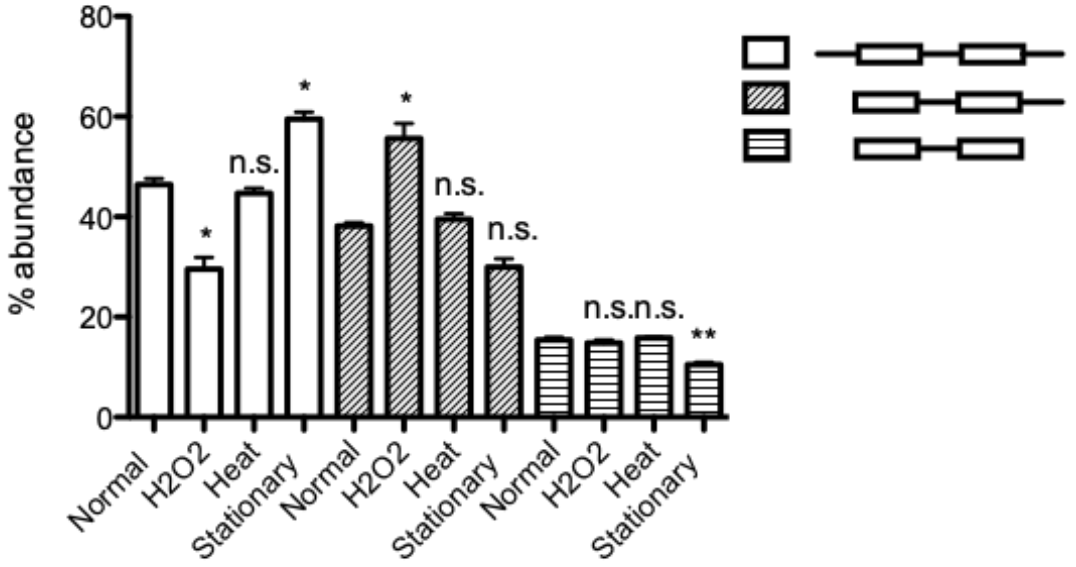

Figure 3.10: Quantification of pre-tRNA Lys^{CUU} processing intermediate abundance from northern blot. The abundance of each pre-tRNA Lys^{CUU} processing intermediate in the Sla1p IP was quantified relative to the total signal (all three processing intermediates) for each cellular condition. Error bars represent mean % abundance of each processing intermediate from three biological replicates +/- SEM. A paired two-tailed t-test was performed for each stress against normal conditions. H_2O_2 stress resulted in significant differences in primary transcript and leader-processed intermediate relative to normal conditions. Stationary phase stress resulted in significant differences in primary transcript and end-processed intermediate relative to normal conditions. Heat stress did not result in altered processing intermediate abundance relative to normal conditions.

Mature tRNA Lys^{CUU} was also probed in order to assess whether the observed effect of cellular stress on pre-tRNA processing resulted in differences in mature levels (**Figure 3.9**) as any observed stalls in pre-tRNA processing could manifest as decreased levels of mature tRNAs. Probing for mature tRNA Lys^{CUU} indicated that this might not be the case, as the mature transcript appeared elevated during stress compared to normal conditions. However, since tRNA half-lives are exceptionally long (hours to days), we also conducted a time course experiment during H_2O_2 stress (**Figure 3.11**). Total RNA was extracted from wild-type and Δ*sla1*

cells prior to H_2O_2 stress, and at 30, 60, and 180 minutes after H_2O_2 stress. Subsequent northern analysis showed an increase in leader-processed pre-tRNA Lys^{CUU} in wild-type cells after 30 minutes of H_2O_2 stress – the same length of time that cells were stressed with H_2O_2 in **Figure 3.9** – and a relative decrease after 60 and 180 minutes, suggesting that at later time points, *S. pombe* cells may somehow adapt in order to restore a more typical distribution of tRNA processing intermediates. Importantly, a similar trend was observed in Δ*sla1* cells, but overall pre-tRNA Lys^{CUU} levels were lower compared to wild-type, suggesting that the effects of H_2O_2 stress on leader-processed pre-tRNA Lys^{CUU} are independent of Sla1p, but overall levels decrease in the absence of Sla1p. Overall, probing for mature tRNA Lys^{CUU} revealed that H_2O_2 stress did not result in altered mature tRNA levels, at least during the time course, despite the observed changes in pre-tRNA processing. Finally, we noticed an apparent decrease in U5 snRNA levels in Δ*sla1* cells, which has not previously been observed in fission yeast, but is reminiscent of proposed functions for La in snRNA processing in budding yeast (Xue et al., 2000)

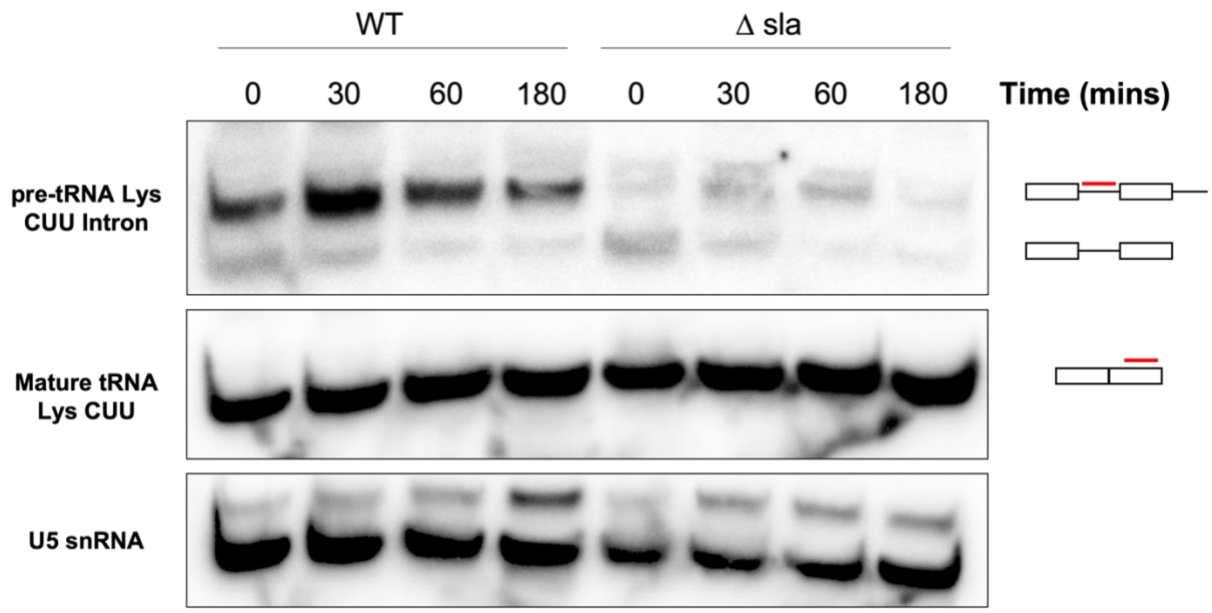

Figure 3.11: Northern blot of H_2O_2 time course in wild-type and Δ*sla1* cells. Total RNA was extracted from wild-type and Δ*sla1* cells prior to 1mM H_2O_2 stress, and after 30, 60, and 180 minutes of H_2O_2 stress. Extracted RNA was resolved on a denaturing urea gel and subjected to northern analysis. RNA species were probed using radiolabelled oligonucleotides that anneal to the targets according to the legend. For both wild-type and Δ*sla1* cells, leader-processed pre-tRNA Lys^{CUU} accumulated after 30 minutes of H_2O_2 stress, followed by a relative decrease after 60 and 180 minutes. Deletion of Sla1p resulted in lower overall levels of leader-processed pre-tRNA Lys^{CUU}. Mature tRNA Lys^{CUU} levels did not appear to be altered during stress. Results from one biological replicate.

3.7 Assessment of Sla1p expression and IP efficiency during stress

Given Sla1p's well-established role in pre-tRNA processing, we sought to determine the extent of Sla1p's involvement in the altered Sla1p-dependent pre-tRNA processing observed during stress. In order to address this, input and IP samples from Sla1p IPs conducted under the chosen cellular conditions were assessed via western blot (**Figure 3.12A**). To assess Sla1p expression during stress, Sla1p levels in stress inputs were normalized to β-actin and quantified relative to normal conditions (**Figure 3.12B**). While there were no significant changes in Sla1p

expression during heat stress, both oxidative and stationary phase stress resulted in increased Sla1p expression. Exposure to H_2O_2 led to nearly a 2-fold increase in Sla1p, while Sla1p overexpression was even less during stationary phase stress. Next, Sla1p IP efficiency was measured by the ratio of Sla1p signal in the Sla1p IP/input, and quantified relative to normal conditions (**Figure 3.12C**). As with Sla1p expression, there were no significant differences in Sla1p IP efficiency during heat stress. Interestingly, while oxidative and stationary phase stress resulted in increased Sla1p expression, Sla1p IP efficiencies were not correspondingly increased during these stresses. Oxidative stress did not significantly affect Sla1p IP efficiency, while stationary phase stress resulted in decreased Sla1p efficiency compared to normal conditions. Altogether, these data do not reveal apparent connections between Sla1p expression and/or IP efficiency during stress, and altered pre-tRNA processing during stress. More detailed discussion is provided in chapter 4.

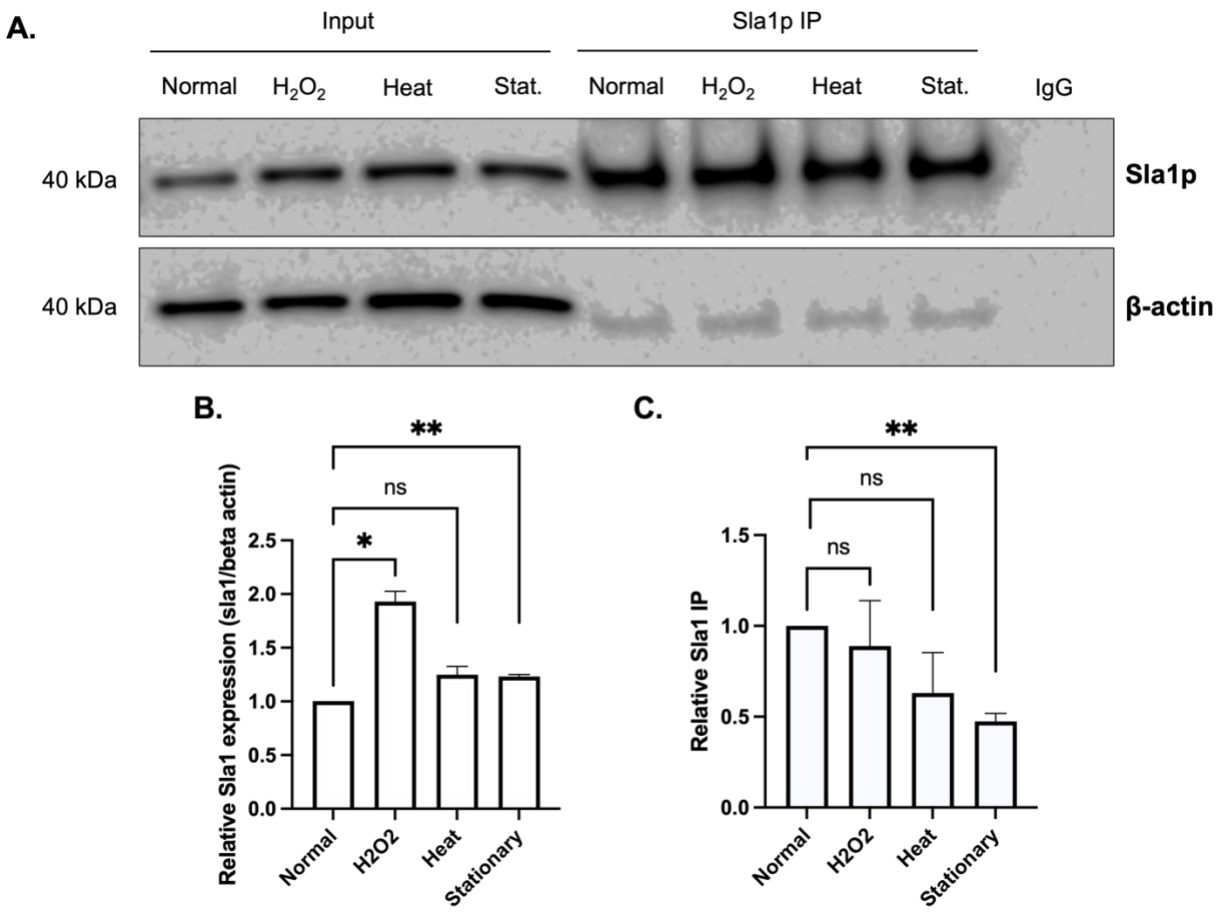

Figure 3.12: Assessment of Sla1p expression and IP efficiency during cellular stress. Endogenous Sla1p was immunoprecipitated from wild-type *S. pombe* cells under normal, and stress conditions using AB2597. Inputs and IP samples were subjected to western analysis using AB2596 (A). An IP conducted with non-immune rabbit IgG from normally grown cells was included as a negative control. β-actin was probed as a loading control. Relative changes in Sla1p expression during stress were quantified by comparing Sla1p signal in inputs relative to β-actin (B). Relative changes in Sla1p IP efficiency under stress were quantified by comparing IP/input ratios for each stress relative to normal conditions (C). Error bars represent mean ratio from three biological replicates +/- SEM. A paired two-tailed t-test was performed for each stress against normal conditions. Sla1p expression was increased during oxidative and stationary phase stress. Sla1p IP efficiency was decreased during stationary phase stress.

3.8 Sla1p does not influence reduced growth in response to H_2O_2 stress

In order to test the possible function of Sla1p in H_2O_2 stress over longer time frames, survival assays were performed in order to determine whether the observed changes in pre-

tRNA processing were linked to *sla1* function and cellular survival. Assays were conducted in both wild-type and Δ*sla1* cells to assess the role of Sla1p during H_2O_2 stress. Serial dilutions of cells +/- *sla1* were spotted on YES agar plates in the presence or absence of H_2O_2 (**Figure 3.13**). Cells spotted on 1 mM H_2O_2 exhibited slightly decreased survival compared to unstressed conditions, while no growth at all was noted in the presence of 2 mM H_2O_2 (image not shown). Additionally, there were no noticeable differences in sensitivity to H_2O_2 +/- *sla1*, suggesting that Sla1p does not play a role in the *S. pombe* response to oxidative stress.

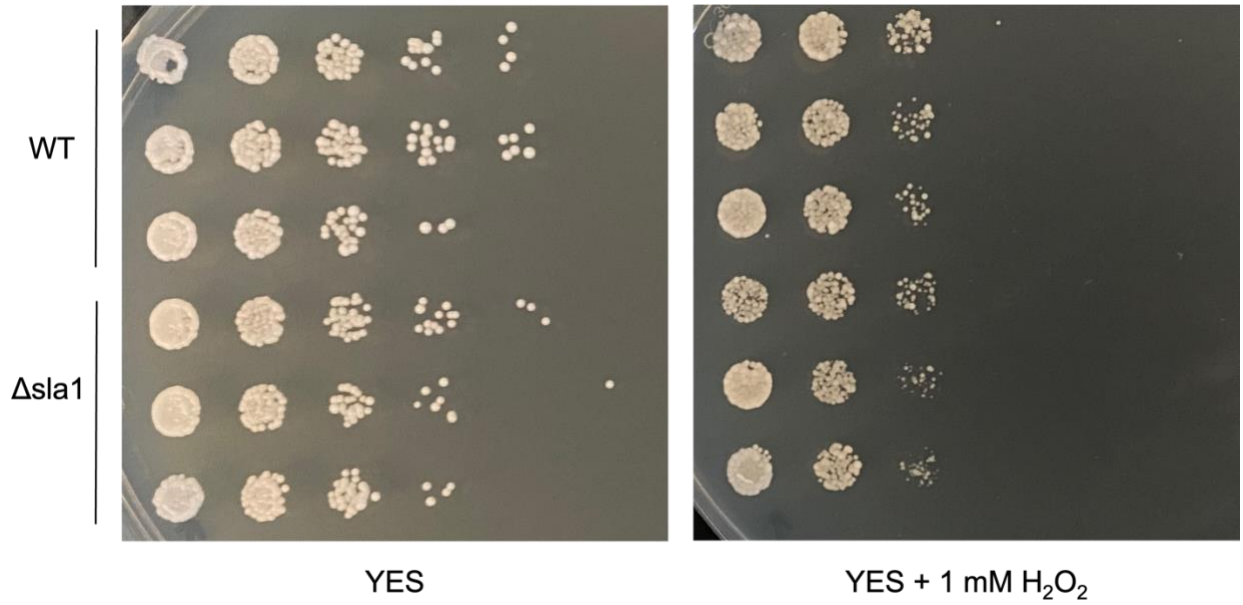

Figure 3.13: H_2O_2 stress spotting assay. Serial dilutions of wild-type (WT) and *Δsla1* cells from three biological replicates were spotted on YES agar plates containing either 0, 1, or 2 mM H_2O_2. There were no significant differences in growth between WT and *Δsla1* cells in the absence of H_2O_2. Survival decreased slightly in 1 mM H_2O_2 and presence of Sla1p was unable to rescue growth. No growth was observed in the presence of 2 mM H_2O_2 (not pictured).

Although only minor growth defects were observed during H_2O_2 stress, it was noted that colonies on the more dilute spots on the plate containing 1 mM H_2O_2 were smaller in size than unstressed colonies, suggesting slower growth. To gain a closer view of survival under H_2O_2

stress, single colonies were spread over larger areas (**Figure 3.13**). As before, cells did not survive in the presence of 2 mM H_2O_2, and growth was not rescued in the presence of Sla1p. Growth was not impaired in the presence of 1 mM H_2O_2 and there were no noticeable differences +/- Sla1p. Altogether, these results suggest decreased cell growth in response to H_2O_2 stress is not influenced by the presence of Sla1p.

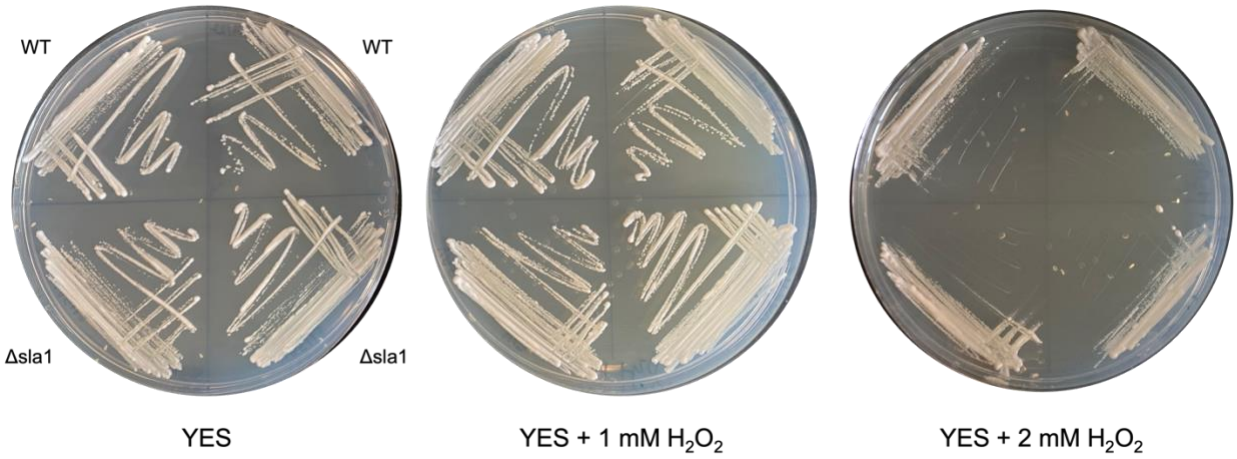

Figure 3.14: H_2O_2 stress does not affect survival. Two colonies each of wild-type (WT) and Δ*sla1* strains were picked and streaked on YES agar plates containing either 0, 1, or 2 mM H_2O_2. The orientation of each plate is consistent with the quadrant labels for the YES plate. No notable growth defects were observed in 1 mM H_2O_2 compared to without, as well as in the absence of Sla1p. A notable reduction of growth was observed in 2 mM H_2O_2 compared to without that could not be rescued with Sla1p.

CHAPTER 4: DISCUSSION

This thesis aimed to further our understanding of the mechanisms behind the RNA chaperone activity of the *S. pombe* La protein homolog. A key question within the RNA chaperone research niche is whether these proteins can discriminate between potential RNA substrates based on how closely their structure resembles the native fold. It is predicted that RNAs whose structure deviates most from the native fold would benefit most from intervention by RNA chaperones. In the context of the La protein, whose dual role in pre-tRNA processing is well-characterized, substrate discrimination for chaperone activity would benefit misfolded RNAs while maintaining processing efficiency for natively folded RNAs that do not require chaperone intervention. Previous work in our lab concluded that Sla1p does not discriminate between pre-tRNA substrates whose fold differs based on the presence or absence of a *single* stabilizing post-transcriptional modification (Vakiloroayaei et al., 2017). This thesis expanded on this work by querying Sla1p's *entire* interactome with TGIRT-seq during cellular stresses expected to have a *global* negative impact on RNA structure and stability.

Ultimately, we aimed to identify any RNA substrates, but particularly pre-tRNAs, whose association with Sla1p was altered during stress compared to normal conditions. In order to achieve this, we developed a workflow that began with the generation of an antibody against Sla1p that was used to IP endogenous Sla1p-RNA complexes from variably stressed *S. pombe* cells. Prior to TGIRT-seq analysis, our antibody was optimized for use in immunodetection assays, and our workflow was validated for the detection of Sla1p-associated pre-tRNAs. Our workflow directly addressed our research question and revealed novel stress-induced alterations to pre-tRNA processing in *S. pombe*.

4.1 Comprehensive assessment of custom α-Sla1p antibodies

The custom α-Sla1p antibodies were validated and optimized for immunodetection using western analysis (**Figure 3.3**). When validating antibodies for western blot, the recommended starting dilution is usually 1:1000 (Koch et al., 2018). Additionally, prior to the generation of the custom α-Sla1p antibody, detection of Sla1p in our lab was conducted using a 1:10,000 dilution of α-Protein A antibody against endogenous Protein A-tagged Sla1p. Therefore, detection of Sla1p using our antibody at concentrations equal to those of commercial tag-specific antibodies suggests high antigen affinity. Although most western blots were conducted using a 1:2000 primary antibody dilution, for the purpose of conserving antibody stock, future western blots for Sla1p detection can be conducted with greater primary antibody dilutions.

As previously highlighted, tag-specific antibodies are used to detect epitope-tagged proteins when an antibody targeting the protein of interest is not available. Although epitope tags are commonly employed in molecular biology for various purposes, their use in an interactome-based investigation such as this one should be cautioned. Epitope tags may interfere with protein function and importantly, they may interact with their own cohorts of RNAs in the cell that may skew results. While tag-specific antibodies are commercially produced, detection of tagged proteins can also be variable or fail altogether (Debeljak et al., 2006). Although there are ways to control for and work around these concerns, not using tag-specific antibodies eliminates them altogether and simplifies the experimental workflow.

The production of two unique mixtures of custom polyclonal antibody also allows for comparison between the two regarding their uses in immunodetection assays. As observed in **Figure 3.3**, western blots conducted with AB2597 demonstrate detection of a non-specific protein greater in molecular weight (50 kDa) than Sla1p (approximately 40 kDa). Worth noting is that this protein is detectable in prepared cell lysates and not in the purified Sla1p sample loaded in lane 9, suggesting that it is an endogenous *S. pombe* protein that bears partial sequence similarity to Sla1p. In IPs conducted with AB2597, the non-specific protein is detected in the input and FT lanes, but not in the IP elution (**Figures 3.4 and 3.5**). Since the non-specific protein is not immunoprecipitated by AB2597, it is likely that AB2597 recognizes it only in its denatured state, and not its physiological folded conformation. From this we can extrapolate that the epitope on the protein recognized by AB2597 may remain buried within the inside of the folded protein under physiological conditions and therefore likely consists of hydrophobic amino acid residues. Interestingly, the non-specific protein is not detected in western blots conducted with AB2596, implying greater antigen specificity for AB2596 versus AB2597. As a result, the IPs conducted ahead of sequencing were conducted with AB2597 and western validations were conducted with AB2596.

Ultimately, the generation of an antibody targeting Sla1p was a pioneering method in our lab that allowed us to avoid many confounding issues from working within tagged yeast strains. In this work we optimized our antibody in immunodetection assays, and demonstrated its success in RNA immunoprecipitation experiments for high-throughput sequencing of Sla1p's RNA interactome.

4.2 Sla1p does not discriminate among substrates based on fold

Analysis of TGIRT-seq data was conducted by our collaborators at L'Université de Sherbrooke. Although IgG mock IPs were conducted in parallel to Sla1p IPs, RNA isolated from IgG IPs were not sequenced as it was suspected that there was not sufficient RNA for the sequencing reaction. IgG lanes in northern (**Figure 3.9**) and western (**Figure 3.12**) analyses from samples prepared with the same workflow were clear of any RNA and Sla1p protein, respectively. This suggests high antibody-antigen specificity and justified our choice. After filtering genes with low and variable reads among replicates, our collaborators used differential expression analysis to identify targets whose interaction with Sla1p was altered during stress (**Figure 3.8**). From this analysis, a ratio of ratios (RoR) = 1 indicated that the RNA in question interacted with Sla1p equally during stress as during normal conditions. Thus, RoR > 1 indicated that the RNA in question interacted more with Sla1p during stress, presumably due to decreased stability during stress and necessity of Sla1p intervention. In contrast, RoR < 1 indicated the opposite; that the RNA in question was more lowly associated with Sla1p during stress. The sequencing analysis indicated that there were no pre-tRNAs that exhibited significantly increased interaction with Sla1p during stress, suggesting that Sla1p does not discriminate among targets based on fold, presuming that some version of misfolding occurs during stress conditions. These results are consistent with previous work that showed that other RNA chaperone proteins, including Sla1p from our own lab, promiscuously interact with tRNAs regardless of fold (Huang et al., 2006; Keffer-Wilkes et al., 2016; Vakiloroayaei et al., 2017). In contrast to these other studies, our work captured the global *in vivo* interactome of Sla1p, rather than focusing on select substrates and/or using *in vitro* interaction studies. As

previously mentioned, Sla1p's lack of substrate discrimination has implications in pre-tRNA maturation and turnover. Since Sla1p is limiting in the cell compared to pre-tRNAs (Huang et al., 2005), structurally aberrant pre-tRNAs are not as likely to receive chaperone intervention from Sla1p before they are degraded via nuclear surveillance. This is supported by observed decreased pre-tRNA levels in Δ*sla1* cells (**Figure 3.11**). As well, Sla1p may bind correctly folded pre-tRNAs with just as much affinity and interfere with their processing efficiency. While it is known that Sla1p's interaction with the uridylate trailer drives the order of 3' end processing of pre-tRNAs, Sla1p-independent pre-tRNA processing ultimately leads to the same mature product. Thus, since a natively folded pre-tRNA does not *require* chaperone intervention from Sla1p, substrate discrimination would benefit misfolded pre-tRNAs without clear disadvantages to the processing of natively folded pre-tRNAs.

While significant substrate discrimination was not observed for pre-tRNAs, oxidative stress resulted in significantly altered interaction with Sla1p for a subset of mRNAs (**Figure 3.8**). Interestingly, mRNAs whose interaction with Sla1p increased during oxidative stress encoded ribosomal proteins, and those with decreased interaction with Sla1p were mitochondrially encoded mRNAs. At this time, reasons for altered interaction between Sla1p and these mRNA cohorts during oxidative stress remain unclear, especially given Sla1p's preference for RNAP III-encoded transcripts and our size selection method. While full-length mRNAs should have been excluded from our sequencing samples via gel extraction, it is possible that these reads correspond to mRNA degradation products. It has been reported that damaged RNA can be degraded by exoribonucleases that bind 8-OHG oligonucleotides with specificity and higher affinity than undamaged RNA (Hayakawa et al., 2001; Li et al., 2006). Additionally, human La

has been shown to promote the cap-independent translation of mRNAs via contacts to the poly(A) tail (Vinayak et al., 2018), and the budding yeast La homolog was previously found to interact with ribosomal protein mRNAs (Inada & Guthrie, 2004). Validation of altered Sla1p interaction with these mRNAs during H_2O_2 stress was attempted via qRT-PCR on a preliminary basis and remains an interesting avenue for future work.

Overall, we demonstrated an experimental workflow that successfully addressed our research question in a direct and physiologically relevant manner. Our data indicate that like other RNA chaperone proteins, Sla1p does not discriminate among natively folded and structurally aberrant substrates for binding. Limitations to our work are presented in section 4.4 along with recommendations for future studies.

4.3 Novel stress-dependent perturbations to pre-tRNA processing in *S. pombe*

Northern analyses conducted to validate the results from sequencing analysis provided novel insights into pre-tRNA processing in *S. pombe* during stress. Using intron-specific probes for various pre-tRNAs we observed altered association of pre-tRNA processing intermediates with Sla1p during H_2O_2 and stationary phase stress (**Figure 3.9**). The effect was most prominent for pre-tRNA Lys^{CUU}. Under normal cellular conditions, Sla1p interacted most with nascent, unprocessed pre-tRNA Lys^{CUU}, followed by the 5' end-processed intermediate, and then the fully processed intermediate. This is consistent with Sla1p's uridylate-dependent binding mode and established role in pre-tRNA processing. During H_2O_2 stress, this distribution was shifted towards most interaction with the 5' end-processed intermediate. During stationary phase

stress, the distribution of processing intermediates that interacted with Sla1p were the same as those in the unstressed cells yet signal for the nascent transcript was much more enriched. Similar results were obtained when probing for other intron-containing pre-tRNAs such as Ser^{UGA} and Val^{AAC}. Interestingly, for an intron-less tRNA, Asn^{GUU}, the 5' end-processed intermediate was the most abundant associated with Sla1p during *both* H_2O_2 and stationary phase stress. Analysis from total input RNA of H_2O_2 stressed cells revealed that 5' end-processed pre-tRNA Lys^{CUU} was also increased in abundance compared to unstressed cells. Importantly, the nascent unprocessed intermediate of pre-tRNA Lys^{CUU} was not observable in input lanes, as well as precursors for the other tRNA species tested. This is likely due to the relatively short half-life of pre-tRNAs as well as limited resolution of northern blots. Thus, due to the intact polyuridylate tail of these species, they associated as expected with Sla1p during the IP and became clearly discernible via northern analysis.

To further support the notion that H_2O_2 stress causes altered pre-tRNA processing, the same leader-processed pre-tRNA Lys^{CUU} intermediate was overly present in total RNA inputs after 30 minutes of stress during the time course (**Figure 3.11**). While there was less overall pre-tRNA Lys^{CUU} present in the Δ*sla1* strain throughout the time course, the leader-processed intermediate was similarly more abundant after 30 minutes of H_2O_2 stress. This result is consistent was Sla1p's role in supporting pre-tRNA stability, and suggests that altered processing during stress occurs independently from the presence of Sla1p. Interestingly, after 60 and 180 minutes of H_2O_2 stress, leader-processed pre-tRNA Lys^{CUU} abundance returned to levels comparable to unstressed conditions. These data suggest that altered pre-tRNA

processing may be a response to only acute oxidative stress, and that the cell adapts to prolonged oxidative stress by resolving processing defects.

Overall, our work has revealed stress-induced alterations to the processing of some pre-tRNA species in *S. pombe*. These results are reminiscent of those famously elucidated in *S. cerevisiae* (**Figure 1.6**) but are of a different pattern. To our knowledge, such effects have not been demonstrated in fission yeast. During H_2O_2 stress, leader-processed intermediates may accumulate due to either increased rates of 5' leader processing or inhibited/stalled 3' trailer cleavage. It was recently reported that H_2O_2 stress in *Streptococcus oligofermentans* causes oxidative degradation of RNase Z, the endonuclease responsible for trailer cleavage (Dong et al., 2021). The authors also reported an accumulation of trailer-containing pre-tRNA species and a decrease in mature tRNAs during H_2O_2 stress. It is therefore plausible that *S. pombe* RNase Z is also sensitive to oxidative damage, leading to a bottleneck of leader-processed pre-tRNA species during H_2O_2 stress. Although not clear from northern analysis, tRNA transcription could be upregulated during nutrient starvation as a means of redistributing energy for essential processes, leading to increased levels of nascent pre-tRNAs. Alternatively, this bottleneck could also result from inhibited 5' leader processing by RNase P.

4.4 Limitations and future directions

This study had two main limitations. First, it was not shown that pre-tRNAs were misfolded during the chosen cellular stresses. Rather, it was presumed based on literature that cellular stress led to overall reduced structural stability for RNAs. A recent study has introduced

a method termed ‘tRNA structure-seq’ that accurately determines the structure of tRNAs *in vivo* using chemical probing coupled to high-throughput sequencing (Yamagami et al., 2022). Thus, this work can be strengthened in the future by validating loss of 3D structure during stress using *in vivo* methods such as tRNA structure-seq.

The second key limitation of our study stems from our sequencing analysis pipeline. We sought to address our research question in the most direct and straightforward way. Consequently, all pre-tRNA processing intermediates were viewed as a single pre-tRNA species during the sequence alignment step of analysis. Thus, although our northern analyses depicted altered interaction of the different processing intermediates with Sla1p, this was not reflected in the sequencing analysis. We therefore plan to re-analyze the sequencing data, separating the different pre-tRNA processing intermediates, to determine whether the observed stress-dependent alterations to pre-tRNA processing are reflected in the sequencing data. This more precise analysis may also address any changes in nascent pre-tRNA levels during stress that were not clear during northern analysis due to reduced resolution and depth. Importantly, this analysis may reveal other pre-tRNA species that experience similar or different processing alterations during stress than those presented here, and may address the universality of our observation.

Finally, we also plan to address the causes for altered pre-tRNA processing during cellular stress. As highlighted earlier, a plausible explanation for the accumulation of leader-processed pre-tRNAs during H_2O_2 stress is the oxidative degradation of RNase Z. To address this, RNase Z abundance can be measured via western blot from whole-cell lysates of unstressed and H_2O_2-stressed cells. Increased accumulation of unprocessed pre-tRNAs during

nutrient starvation may arise due to increased transcription by RNAP III or by decreased RNase P activity. The possibility of increased transcription during stress can be addressed by chromatin immunoprecipitation coupled to sequencing (ChIP-seq). Using ChIP-seq, RNAP III occupancy at tRNA genes can be quantified, and tRNA transcription can therefore be compared during normal conditions and nutrient starvation.

REFERENCES

Agris, P. F., Vendeix, F. A. P., & Graham, W. D. (2007). tRNA's wobble decoding of the genome: 40 years of modification. *Journal of Molecular Biology*, *366*(1), 1–13. https://doi.org/10.1016/J.JMB.2006.11.046

Alfano, C., Sanfelice, D., Babon, J., Kelly, G., Jacks, A., Curry, S., & Conte, M. R. (2004). Structural analysis of cooperative RNA binding by the La motif and central RRM domain of human La protein. *Nature Structural & Molecular Biology 11:4*, *11*(4), 323–329. https://doi.org/10.1038/nsmb747

Arimbasseri, A. G., Blewett, N. H., Iben, J. R., Lamichhane, T. N., Cherkasova, V., Hafner, M., Maraia, R. J., & Hopper, A. (2015). RNA Polymerase III Output Is Functionally Linked to tRNA Dimethyl-G26 Modification. *PLoS Genetics 11(12),* https://doi.org/10.1371/journal.pgen.1005671

Arimbasseri, A. G., Rijal, K., & Maraia, R. J. (2013). Transcription termination by the eukaryotic RNA polymerase III. *Biochimica et Biophysica Acta 1829(3-4): 318-330,* https://doi.org/10.1016/j.bbagrm.2012.10.006

Bayfield, M. A., & Maraia, R. J. (2009). Precursor-product discrimination by La protein during tRNA metabolism. *Nature Structural and Molecular Biology 16(4):430-7,* https://doi.org/10.1038/nsmb.1573

Becskei, A., & Rahaman, S. (2022). The life and death of RNA across temperatures. *Computational and Structural Biotechnology Journal*, *20*, 4325. https://doi.org/10.1016/J.CSBJ.2022.08.008

Berg, M. D., & Brandl, C. J. (2021). Transfer RNAs: diversity in form and function. *RNA Biology*, *18*(3), 316–339. https://doi.org/10.1080/15476286.2020.1809197

Boivin, V., Reulet, G., Boisvert, O., Couture, S., Elela, S. A., & Scott, M. S. (2020). Reducing the structure bias of RNA-Seq reveals a large number of non-annotated non-coding RNA. *Nucleic Acids Research*, *48*(5), 2271. https://doi.org/10.1093/NAR/GKAA028

Bolger, A. M., Lohse, M., & Usadel, B. (2014). Genome analysis Trimmomatic: a flexible trimmer for Illumina sequence data. *Bioinformatics 30*(15), 2114–2120, https://doi.org/10.1093/bioinformatics/btu170

Chakshusmathi, G., Kim, S. Do, Rubinson, D. A., & Wolin, S. L. (2003). A La protein requirement for efficient pre-tRNA folding. *EMBO Journal*, *22*(24), 6562–6572. https://doi.org/10.1093/EMBOJ/CDG625

Chamberlain, J. R., Lee, Y., Lane, W. S., & Engelke, D. R. (1998). Purification and characterization of the nuclear RNase P holoenzyme complex reveals extensive subunit overlap with RNase MRP. *Genes and Development 12(11): 1678-90*. http:// doi: 10.1101/gad.12.11.1678

Chan, C. T. Y., Dyavaiah, M., DeMott, M. S., Taghizadeh, K., Dedon, P. C., & Begley, T. J. (2010). A quantitative systems approach reveals dynamic control of tRNA modifications during cellular stress. *PLoS Genetics*, *6*(12), 1–9. https://doi.org/10.1371/JOURNAL.PGEN.1001247

Chan, E. K. L., Sullivan, K. F., & Tan, E. M. (1989). Ribonucleoprotein SS-B/La belongs to a protein family with consensus sequences for RNA-binding. *Nucleic Acids Research*, *17*(6), 2233. https://doi.org/10.1093/NAR/17.6.2233

Chernyakov, I., Whipple, J. M., Kotelawala, L., Grayhack, E. J., & Phizicky, E. M. (2008). Degradation of several hypomodified mature tRNA species in Saccharomyces cerevisiae is mediated by Met22 and the 5-3 exonucleases Rat1 and Xrn1. *Genes and Development 22(10): 1369-80*. https://doi.org/10.1101/gad.1654308

Cozen, A. E., Quartley, E., Holmes, A. D., Hrabeta-Robinson, E., Phizicky, E. M., & Lowe, T. M. (2015). ARM-seq: AlkB-facilitated RNA methylation sequencing reveals a complex landscape of modified tRNA fragments. *Nature Methods*, *12*(9), 879–884. https://doi.org/10.1038/NMETH.3508

Debeljak, N., Feldman, L., Davis, K. L., Komel, R., & Sytkowski, A. J. (2006). Variability in the Immunodetection of His-tagged Recombinant Proteins. *Analytical Biochemistry*, *359*(2), 216. https://doi.org/10.1016/J.AB.2006.09.017

Deschamps-Francoeur, G., Boivin, V., Elela, S. A., & Scott, M. S. (2019). *CoCo: RNA-seq read assignment correction for nested genes and multimapped reads*. https://doi.org/10.1093/bioinformatics/btz433

Dobin, A., & Gingeras, T. R. (2016). Optimizing RNA-seq mapping with STAR. *Methods in Molecular Biology*, *1415*, 245–262. https://doi.org/10.1007/978-1-4939-3572-7_13/COVER

Doetsch, M., Schroeder, R., & Fürtig, B. (2011). Transient RNA-protein interactions in RNA folding. *FEBS Journal*, *278*(10), 1634–1642. https://doi.org/10.1111/J.1742-4658.2011.08094.X

Dong, G., Chakshusmathi, G., Wolin, S. L., & Reinisch, K. M. (2004). Structure of the La motif: a winged helix domain mediates RNA binding via a conserved aromatic patch. *The EMBO Journal*, *23*(5), 1000. https://doi.org/10.1038/SJ.EMBOJ.7600115

Dong, Y., Tong, H., Hu, Q., & Dong, X. (2021). RNase Z Oxidative Degradation Impedes tRNA Maturation and is Involved in Streptococcal Translation Regulation in Response to Oxidative Stress. *Microbiology Spectrum*, *9*(2). https://doi.org/10.1128/SPECTRUM.01167-21

Draper, D. E. (1992). The RNA-Folding Problem. *Accounts of Chemical Research*, *25*(4), 201–207. https://doi.org/10.1021/AR00016A005/ASSET/AR00016A005.FP.PNG_V03

Fafard-Couture, É., Bergeron, D., Couture, S., Abou-Elela, S., & Scott, M. S. (2021). Annotation of snoRNA abundance across human tissues reveals complex snoRNA-host gene relationships. *Genome Biology*, *22*(1), 1–24. https://doi.org/10.1186/S13059-021-02391-2/FIGURES/6

Fok, V., Friend, K., & Steitz, J. A. (2006). Epstein-Barr virus noncoding RNAs are confined to the nucleus, whereas their partner, the human La protein, undergoes nucleocytoplasmic shuttling. *The Journal of Cell Biology*, *173*(3), 319. https://doi.org/10.1083/JCB.200601026

Foretek, D., Wu, J., Hopper, A. K., & Boguta, M. (2016). Control of Saccharomyces cerevisiae pre-tRNA processing by environmental conditions. *RNA 22(3): 339-349*. https://doi.org/10.1261/rna.054973.115

Gudipati, R. K., Xu, Z., Lebreton, A., Séraphin, B., Steinmetz, L. M., Jacquier, A., & Libri, D. (2012). Extensive degradation of RNA precursors by the exosome in wild-type cells. *Molecular Cell*, *48*(3), 409–421. https://doi.org/10.1016/J.MOLCEL.2012.08.018

Hayakawa, H., Kuwano, M., & Sekiguchi, M. (2001). Specific Binding of 8-Oxoguanine-Containing RNA to Polynucleotide Phosphorylase Protein. *Biochemistry*, *40*(33), 9977–9982. https://doi.org/10.1021/BI010595Q

Herschlag, D. (1995). RNA chaperones and the RNA folding problem. *Journal of Biological Chemistry*, *270*(36), 20871–20874. https://doi.org/10.1074/JBC.270.36.20871

Hopper, A. K., & Phizicky, E. M. (2003). tRNA transfers to the limelight. *Genes and Development, 17(2): 162-80*. https://doi.org/10.1101/gad.1049103

Huang, H.-Y., & Hopper, A. K. (2016). Multiple Layers of Stress-Induced Regulation in tRNA Biology. *Life (Basel), 6(2): 16*. https://doi.org/10.3390/life6020016

Huang, X., & Tang, J. (2020). Human La Protein: An RNA-Binding Protein Involved in Ovarian Cancer Development and Multidrug Resistance. *OncoTargets and Therapy*, *13*, 10721. https://doi.org/10.2147/OTT.S269983

Huang, Y., Bayfield, M. A., Intine, R. V., & Maraia, R. J. (2006). Separate RNA-binding surfaces on the multifunctional La protein mediate distinguishable activities in tRNA maturation. *Nature Structural & Molecular Biology 2006 13:7*, *13*(7), 611–618. https://doi.org/10.1038/nsmb1110

Huang, Y., Intine, R. V., Mozlin, A., Hasson, S., & Maraia, R. J. (2005). Mutations in the RNA Polymerase III Subunit Rpc11p That Decrease RNA 3′ Cleavage Activity Increase 3′-Terminal Oligo(U) Length and La-Dependent tRNA Processing. *Molecular and Cellular Biology*, *25*(2), 621. https://doi.org/10.1128/MCB.25.2.621-636.2005

Inada, M., & Guthrie, C. (2004). Identification of Lhp1p-associated RNAs by microarray analysis in Saccharomyces cerevisiae reveals association with coding and noncoding RNAs. *Proceedings of the National Academy of Sciences of the United States of America*, *101*(2), 434. https://doi.org/10.1073/PNAS.0307425100

Ivanyi-Nagy, R., Lavergne, J.-P., Gabus, C., Ficheux, D., & Darlix, J.-L. (2008). RNA chaperoning and intrinsic disorder in the core proteins of Flaviviridae. *Nucleic Acids Research*, *36*(3), 712–725. https://doi.org/10.1093/nar/gkm1051

Kadaba, S., Krueger, A., Trice, T., Krecic, A. M., Hinnebusch, A. G., & Anderson, J. (2004). Nuclear surveillance and degradation of hypomodified initiator tRNAMet in S. cerevisiae. *Genes & Development*, *18*(11), 1227–1240. https://doi.org/10.1101/GAD.1183804

Kadaba, S., Wang, X., & Anderson, J. T. (2006). Nuclear RNA surveillance in Saccharomyces cerevisiae: Trf4p-dependent polyadenylation of nascent hypomethylated tRNA and an aberrant form of 5S rRNA. *RNA*, *12*(3), 508. https://doi.org/10.1261/RNA.2305406

Kaliatsi, E. G., Argyriou, A. I., Bouras, G., Apostolidi, M., Konstantinidou, P., Shaukat, A. N., Spyroulias, G. A., & Stathopoulos, C. (2020). Functional and Structural Aspects of La Protein Overexpression in Lung Cancer. *Journal of Molecular Biology*, *432*(24), 166712. https://doi.org/10.1016/J.JMB.2020.11.011

Karaca, E., Weitzer, S., Pehlivan, D., Shiraishi, H., Gogakos, T., Hanada, T., Jhangiani, S. N., Wiszniewski, W., Withers, M., Campbell, I. M., Erdin, S., Isikay, S., Franco, L. M., Gonzaga-Jauregui, C., Gambin, T., Gelowani, V., Hunter, J. V., Yesil, G., Koparir, E., … Lupski, J. R. (2014). Human CLP1 mutations alter tRNA biogenesis, affecting both peripheral and central nervous system function. *Cell*, *157*(3), 636–650. https://doi.org/10.1016/J.CELL.2014.02.058

Keffer-Wilkes, L. C., Reddy Veerareddygari, G., & Kothe, U. (2016). *RNA modification enzyme TruB is a tRNA chaperone*. https://doi.org/10.1073/pnas.1607512113

Kerkhofs, K., Garg, J., Fafard-Couture, É., Abou Elela, S., Scott, M. S., Pearlman, R. E., & Bayfield, M. A. (2022). *Altered tRNA processing is linked to a distinct and unusual La protein in Tetrahymena thermophila*. https://doi.org/10.1038/s41467-022-34796-3

Koch, R. J., Barrette, A. M., Stern, A. D., Hu, B., Bouhaddou, M., Azeloglu, E. U., Iyengar, R., & Birtwistle, M. R. (2018). Validating Antibodies for Quantitative Western Blot Measurements with Microwestern Array. *Scientific Reports 2018 8:1*, *8*(1), 1–10. https://doi.org/10.1038/s41598-018-29436-0

Kong, Q., & Lin, C. (2011). Oxidative damage to RNA: mechanisms, consequences, and diseases. *Cellular and Molecular Life Sciences, 67(11): 1817-1829*. https://doi.org/10.1007/s00018-010-0277-y

Kotik-Kogan, O., Valentine, E. R., Sanfelice, D., Conte, M. R., & Curry, S. (2008). Structural Analysis Reveals Conformational Plasticity in the Recognition of RNA 3 0 Ends by the Human La Protein. *Structure, 16(6): 852-62.* https://doi.org/10.1016/j.str.2008.02.021

Lerner, M. R., & Argetsinger Steitz, J. (1979). Antibodies to small nuclear RNAs complexed with proteins are produced by patients with systemic lupus erythematosus. *Proceedings of the National Academy of Sciences*, *76*(11), 5495–5499. https://doi.org/10.1073/PNAS.76.11.5495

Li, Z., Wu, J., & DeLeo, C. J. (2006). RNA damage and surveillance under oxidative stress. *IUBMB Life*, *58*(10), 581–588. https://doi.org/10.1080/15216540600946456

Love, M. I., Huber, W., & Anders, S. (2014). Moderated estimation of fold change and dispersion for RNA-seq data with DESeq2. *Genome Biology*, *15*(12), 1–21. https://doi.org/10.1186/S13059-014-0550-8/FIGURES/9

Maraia, R. J., & Lamichhane, T. N. (2011). 3′ processing of eukaryotic precursor tRNAs. *Wiley Interdisciplinary Reviews: RNA*, *2*(3), 362–375. https://doi.org/10.1002/WRNA.64

Maraia, R. J., Mattijssen, S., Cruz-Gallardo, I., & Conte, M. R. (2017). The La and related RNA-binding proteins (LARPs): structures, functions, and evolving perspectives. *Wiley Interdisciplinary Reviews: RNA*, *8*(6), e1430. https://doi.org/10.1002/WRNA.1430

Marrella, S. A., Brown, K. A., Mansouri-Noori, F., Porat, J., Wilson, D. J., & Bayfield, M. A. (2019). An interdomain bridge influences RNA binding of the human La protein. *The Journal of Biological Chemistry*, *294*(5), 1529–1540. https://doi.org/10.1074/JBC.RA118.003995

Mattioli, M., & Reichlin, M. (1974). Heterogeneity of RNA protein antigens reactive with sera of patients with systemic lupus erythematosus description of a cytoplasmic nonribosomal antigen. *Arthritis & Rheumatism*, *17*(4), 421–429. https://doi.org/10.1002/ART.1780170413

Murthi, A., Shaheen, H. H., Huang, H. Y., Preston, M. A., Lai, T. P., Phizicky, E. M., & Hopper, A. K. (2010). Regulation of tRNA bidirectional nuclear-cytoplasmic trafficking in Saccharomyces cerevisiae. *Molecular Biology of the Cell*, *21*(4), 639–649. https://doi.org/10.1091/MBC.E09-07-0551

Naeeni, A. R., Conte, M. R., & Bayfield, M. A. (2012). RNA chaperone activity of human La protein is mediated by variant RNA recognition motif. *The Journal of Biological Chemistry*, *287*(8), 5472–5482. https://doi.org/10.1074/JBC.M111.276071

Nottingham, R. M., Wu, D. C., Qin, Y., Yao, J., Hunicke-Smith, S., & Lambowitz, A. M. (2016). RNA-seq of human reference RNA samples using a thermostable group II intron reverse transcriptase. *RNA*, *22*(4), 597–613. https://doi.org/10.1261/RNA.055558.115

Nunomura, A., Chiba, S., Kosaka, K., Takeda, A., Castellani, R. J., Smith, M. A., & Perry, G. (2002). Neuronal RNA oxidation is a prominent feature of dementia with Lewy bodies. *Neuroreport*, *13*(16), 2035–2039. https://doi.org/10.1097/00001756-200211150-00009

Nunomura, A., Perry, G., Pappolla, M. A., Wade, R., Hirai, K., Chiba, S., & Smith, M. A. (1999). RNA Oxidation Is a Prominent Feature of Vulnerable Neurons in Alzheimer's Disease. *The Journal of Neuroscience, 19(6)*: 1959-64. http://doi: 10.1523/JNEUROSCI.19-06-01959.1999

Oeffinger, M., Wei, K. E., Rogers, R., Degrasse, J. A., Chait, B. T., Aitchison, J. D., & Rout, M. P. (2007). Comprehensive analysis of diverse ribonucleoprotein complexes. *Nature Methods, 4(11):* 951-6. https://doi.org/10.1038/NMETH1101

Ørom, U. A., Milanetti, E., Balestra, D., Htet Htet Aung, L., Li, P., Ding, H., Lhh, A., Li, Z., Chen, X., Liu, Z., Ye, W., Li, L., & Qian, L. (2020). Recent Advances: Molecular Mechanism of RNA Oxidation and Its Role in Various Diseases. *Frontiers in Molecular Biosciences, 7: 184*. https://doi.org/10.3389/fmolb.2020.00184

Park, J.-M., Kohn, M. J., Bruinsma, M. W., Vech, C., Intine, R. V, Fuhrmann, S., Grinberg, A., Mukherjee, I., Love, P. E., Ko, M. S., Depamphilis, M. L., & Maraia, R. J. (2006). The Multifunctional RNA-Binding Protein La Is Required for Mouse Development and for the Establishment of Embryonic Stem Cells. *MOLECULAR AND CELLULAR BIOLOGY*, *26*(4), 1445–1451. https://doi.org/10.1128/MCB.26.4.1445-1451.2006

Porat, J., Kothe, U., & Bayfield, M. A. (2021). Revisiting tRNA chaperones: new players in an ancient game. *RNA*, *27*(5), 543. https://doi.org/10.1261/RNA.078428.120

Qin, Y., Yao, J., Wu, D. C., Nottingham, R. M., Mohr, S., Hunicke-Smith, S., & Lambowitz, A. M. (2016). High-throughput sequencing of human plasma RNA by using thermostable group II intron reverse transcriptases. *RNA*, *22*(1), 111–128. https://doi.org/10.1261/RNA.054809.115

Rajkowitsch, L., Chen, D., Stampfl, S., Semrad, K., Waldsich, C., Mayer, O., Jantsch, M. F., Konrat, R., Bläsi, U., & Schroeder, R. (2007). RNA chaperones, RNA annealers and RNA helicases. *RNA Biology*, *4*(3), 118–130. https://doi.org/10.4161/RNA.4.3.5445

Russell, R. (2008). RNA misfolding and the action of chaperones. *Frontiers in Bioscience: A Journal and Virtual Library*, *13*(1), 1. https://doi.org/10.2741/2557

Shaheen, H. H., & Hopper, A. K. (2005). Retrograde movement of tRNAs from the cytoplasm to the nucleus in Saccharomyces cerevisiae. *Proceedings of the National Academy of Sciences of the United States of America*, *102*(32), 11290–11295. https://doi.org/10.1073/PNAS.0503836102

Shan, X., Chang, Y., & Glenn Lin, C. (2007). Messenger RNA oxidation is an early event preceding cell death and causes reduced protein expression. *FASEB Journal : Official Publication of the Federation of American Societies for Experimental Biology*, *21*(11), 2753–2764. https://doi.org/10.1096/FJ.07-8200COM

Stefano, J. E. (1984). Purified lupus antigen la recognizes an oligouridylate stretch common to the 3' termini of RNA polymerase III transcripts. *Cell*, *36*(1), 145–154. https://doi.org/10.1016/0092-8674(84)90083-7

Svenningsen, S. Lo, Kongstad, M., Stenum, T. S., Muñoz-Gómez, A. J., & Sørensen, M. A. (2017). Transfer RNA is highly unstable during early amino acid starvation in Escherichia coli. *Nucleic Acids Research*, *45*(2), 793. https://doi.org/10.1093/NAR/GKW1169

Tanaka, M., & Chock, P. B. (2021). Oxidative Modifications of RNA and Its Potential Roles in Biosystem. *Frontiers in Molecular Biosciences*, *8*, 407. https://doi.org/10.3389/FMOLB.2021.685331/BIBTEX

Teplova, M., Yuan, Y. R., Phan, A. T., Malinina, L., Ilin, S., Teplov, A., & Patel, D. J. (2006). Structural Basis for Recognition and Sequestration of UUUOH 3' Temini of Nascent RNA Polymerase III Transcripts by La, a Rheumatic Disease Autoantigen. *Molecular Cell*, *21*(1), 75. https://doi.org/10.1016/J.MOLCEL.2005.10.027

Thompson, D. M., Lu, C., Green, P. J., & Parker, R. (2008). tRNA cleavage is a conserved response to oxidative stress in eukaryotes. *RNA (New York, N.Y.)*, *14*(10), 2095–2103. https://doi.org/10.1261/RNA.1232808

Tijerina, P., Bhaskaran, H., & Russell, R. (2006). Nonspecific binding to structured RNA and preferential unwinding of an exposed helix by the CYT-19 protein, a DEAD-box RNA chaperone. *Proceedings of the National Academy of Sciences of the United States of America*, *103*(7). www.pnas.orgcgidoi10.1073pnas.0603127103

Vakiloroayaei, A., Shah, N. S., Oeffinger, M., & Bayfield, M. A. (2017). The RNA chaperone La promotes pre-tRNA maturation via indiscriminate binding of both native and misfolded targets. *Nucleic Acids Research*, *45*(19), 11341–11355. https://doi.org/10.1093/NAR/GKX764

Vinayak, J., Marrella, S. A., Hussain, R. H., Rozenfeld, L., Solomon, K., & Bayfield, M. A. (2018). Human La binds mRNAs through contacts to the poly(A) tail. *Nucleic Acids Research*, *46*(8), 4228–4240. https://doi.org/10.1093/nar/gky090

Wang, Q., Xue, H., Li, S., Chen, Y., Tian, X., Xu, X., Xiao, W., & Fu, Y. V. (2017). A method for labeling proteins with tags at the native genomic loci in budding yeast. *PLoS ONE*, *12*(5). https://doi.org/10.1371/JOURNAL.PONE.0176184

Whitney, M. L., Hurto, R. L., Shaheen, H. H., & Hopper, A. K. (2007). Rapid and reversible nuclear accumulation of cytoplasmic tRNA in response to nutrient availability. *Molecular Biology of the Cell*, *18*(7), 2678–2686. https://doi.org/10.1091/MBC.E07-01-0006

Woodson, S. A., Panja, S., & Santiago-Frangos, A. (2018). Proteins that chaperone RNA regulation. *Microbiology Spectrum*, *6*(4). https://doi.org/10.1128/MICROBIOLSPEC.RWR-0026-2018

Xue, D., Rubinson, D. A., Pannone, B. K., Christopher J, Y., & Wolin, S. L. (2000). U snRNP assembly in yeast involves the La protein. *The EMBO Journal*, *19*(7), 1650. https://doi.org/10.1093/EMBOJ/19.7.1650

Yamagami, R., Sieg, J. P., Assmann, S. M., & Bevilacqua, P. C. (2022). Genome-wide analysis of the in vivo tRNA structurome reveals RNA structural and modification dynamics under heat stress. *Proceedings of the National Academy of Sciences of the United States of America*, *119*(25), e2201237119. https://doi.org/10.1073/PNAS.2201237119/SUPPL_FILE/PNAS.2201237119.SD02.XLSX

Yarian, C., Townsend, H., Czestkowski, W., Sochacka, E., Malkiewicz, A. J., Guenther, R., Miskiewicz, A., & Agris, P. F. (2002). Accurate translation of the genetic code depends on tRNA modified nucleosides. *The Journal of Biological Chemistry*, *277*(19), 16391–16395. https://doi.org/10.1074/JBC.M200253200

Yoo, C. J., & Wolin, S. L. (1997). The Yeast La Protein Is Required for the 3' Endonucleolytic Cleavage That Matures tRNA Precursors. *Cell*, *89*, 393–402. http://doi: 10.1016/s0092-8674(00)80220-2

Zheng, G., Qin, Y., Clark, W. C., Dai, Q., Yi, C., He, C., Lambowitz, A. M., & Pan, T. (2015). Efficient and quantitative high-throughput tRNA sequencing. *Nature Methods*, *12*(9), 835–837. https://doi.org/10.1038/NMETH.3478

APPENDIX A

Table S1: Sequences of northern blot probes and corresponding melting temperature (T_m). Membranes were probed at 10°C below the indicated T_m.

Probe	Sequence	T_m (°C)
Pre-tRNA Lys^{CUU} intron	5'-CTT CTG ATA CCA TTC GTA AGA GTC-3'	52.7
Mature tRNA Lys^{CUU}	5'-CTC CCA AGG CGA GAC TCG AAC TCG CAA-3'	65.4
U5 snRNA	5'-CGA CAC CTT ACA AAC GGC TGT TTC TG-3'	56.1
5S rRNA	5'-CCC GGA TTC CCA TGT TGT CTC CAA C-3'	61.6
Pre-tRNA Ser^{CGA} intron	5'-GCC CAT TAG ATG ACT AGA ATA CAG GAT TCA AG-3'	58.2
Pre-tRNA Val^{AAC} intron	5'-GTC TGC GAA CTG TAA ATG TTA AG-3'	52.1
Pre-tRNA Asn^{GUU} trailer	5'-AGA AAA CGG TCA GGG AGG G-3'	56.9

Table S2: Primer and probe sequences used for qRT-PCR analysis.

Oligonucleotide	Sequence
Pre-tRNA Lys^{CUU} Forward	5'-TCT GAC TCT TAT GAT GGT AAT CGA A-3'
Pre-tRNA Ser^{CGA} Forward	5'-GAA TTC CTA CAT TCG TGG CAT-3'
Universal Reverse	PerfeCta® Universal PCR Primer (Quanta Biosciences)
Pre-tRNA Lys^{CUU} Probe	5'-/56-FAM/CGA GTT CGA/ZEN/GTC TCG CCT TGG G/3IABkFQ/-3'
Pre-tRNA Ser^{CGA} Probe	5'-/56-FAM/CA GGT TCA A/ZEN/A TCC TGC TGG TGA CG/3IABkFQ/3'

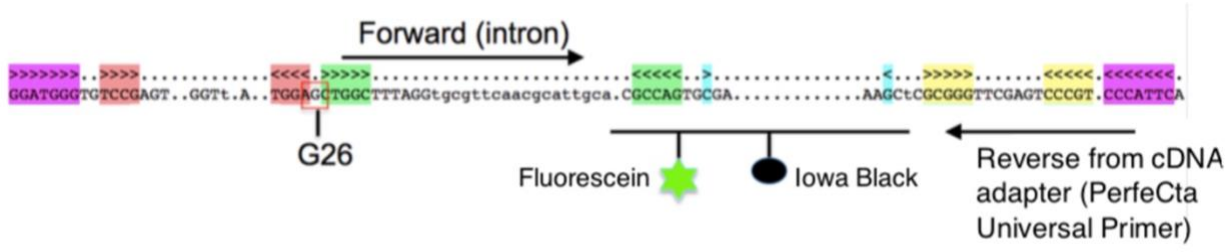

Figure S1: Schematic of probe hybridization for qRT-PCR of pre-tRNAs. qRT-PCR was used to validate the IPs for pre-tRNAs prior to sequencing. RNA from inputs, Sla1p IPs, and IgG IPs were polyadenylated and converted to cDNA using the qScript microRNA cDNA synthesis kit (Quanta Biosciences). Pre-tRNA Lys^{CUU} and Ser^{CGA} were targeted using unique forward primers and TaqMan™ probes, and the PerfeCta® universal reverse primer from the qScript kit. Sample qRT-PCR detection demonstrated above for pre-tRNA Leu^{TAG}. Relative position of probes held constant for all tested pre-tRNAs. Figure adapted from (Vakiloroayaei et al., 2017).

APPENDIX B

Table S3: Differential expression data for statistically significant mRNAs that exhibit altered association with Sla1p under H_2O_2 stress. The table highlights mRNAs for which RoR ≠ 1 and $p_{adj.} \leq 0.05$ during H_2O_2 stress. mRNAs with increased association with Sla1p (RoR > 1) encode ribosomal proteins and those with decreased association with Sla1p (RoR < 1) are mitochondrially encoded.

gene_id	gene_name	H2O2_RoR	pval	padj
SPCC1322.11	rpl2302	3.214704789	0.000774823	0.042063978
SPAC17G6.06	rps2401	3.207445332	0.000409	0.034526054
SPBC2F12.04	rpl1701	2.804793055	0.001161934	0.049398636
SPBC11C11.09c	rpl502	2.662786116	0.000585745	0.040258517
SPCC970.05	rpl3601	2.411359566	0.000726185	0.042063978
SPAC23A1.03	apt1	2.368077655	0.000922926	0.044838306
SPBC839.05c	rps1701	2.298196204	0.000324951	0.030045497
SPAC4G9.16c	rpl901	2.23068723	0.000244268	0.024467465
SPCC1183.08c	rpl101	2.220172748	0.000678382	0.041326991
SPAC1F12.02c	tma19	2.215541169	0.000226316	0.023654946
SPAC23A1.08c	rpl3401	2.137212042	0.000661958	0.041326991
SPAC26A3.04	rpl2002	2.093197884	0.001115586	0.048761258
SPAC24H6.07	rps901	1.937893354	0.000493874	0.03741466
SPMIT.07	atp6	0.150537388	0.000351434	0.031290679
SPMIT.04	cox3	0.137387909	2.42E-05	0.005288639
SPMIT.08	var1	0.083610101	2.64E-06	0.00100831
SPMIT.02	cox1-I1b	0.073734042	1.63E-06	0.000938103
SPMIT.03	cox1-I2b	0.061732318	2.94E-06	0.00100831